NASA-CR-172524
19850018602

NASA Contractor Report 172524

A Gimbal Sizing Analysis
For an IPACS Rotating Assembly

P. R. Burke   and   P. A. Coronato

Allied Bendix Aerospace
Teterboro, New Jersey   07608

NASA

National Aeronautics and
Space Administration

Langley Research Center
Hampton, Virginia 23665

Table of Contents

N85-26913#

List of Figures

List of Tables

1.0 Introduction

Integrated Power/Attitude Control Systems, (IPACS), were investigated in the early 1970's to determine if the dual functions of electrical power storage and spacecraft attitude control could be efficiently integrated into a single package. It was found that a flywheel could be run up and down in speed to store and discharge electrical power, while simultaneously being torqued about a gimbal axis to perform spacecraft attitude control.

An IPACS inner gimbal assembly (IGA), was designed and built by Rockwell International and described in NASA CR-172317 (Reference 1). This IGA incorporates a constant stress titanium rotor, dual motor/generators utilizing high efficiency rare earth magnets, and heat pipes within the rotor to cool the spin bearings. The IGA will store and discharge 2.5 kilowatts of power over a 90 minute earth orbit cycle. When the spacecraft is in the sun lit portion of its orbit, electrical energy generated by solar arrays is stored as kinetic energy by accelerating the rotor up to 35000 rpm. Later on, during the night time of the orbit, the stored energy is recovered through the generators as the rotor is spun down to 17500 rpm. Torquing this IGA at 0.019 radians per second develops 27 N.m. (20 ft.lbs.) of output torque, satisfying the attitude control requirements of the contemplated mission.

The scope of the task performed by Bendix Guidance Systems Division was to review the existing IGA design and produce a preliminary design for the gimballing assembly. An extensive reanalysis of all major components of the IPACS IGA was required to validate the integrity of the present design under a gimballing environment. This report presents the Phase I results of the gimbal sizing analysis performed to complete the IPACS concept and discusses the merit of the overall design in light of today's state of the art techniques and applications. Certain recommendations-redesigns are included to give the existing hardware a maturity necessary for a STS launch and reliable in-orbit operation. Phase II tasks currently being performed include the design of a bellville washer preload system, the use of Custom 455 stainless steel as the rotor material, and an update of the system response analysis.

2.0 General Description

The current IPACS design may be divided into two distinct sections: the existing experimental inner gimbal assembly (IGA), and the conceptual exterior gimballing assembly. A brief description of each of these is presented in the following sections.

2.1 Inner Gimbal Assembly (IGA)

The IPACS IGA has six major subassemblies: the rotor, the dual motor/generator units, the spin bearings, their lubrication systems, the preload mechanism and the inner gimbal (see Figure 1).

The rotor is machined from a solid forging of 6Al-4V titanium. The high strength to density relationship of this alloy translates into high power storage per weight for the flywheel. A "constant stress" criterion was used to develop the contour of the rotor. Consequently, the large shape factor of the rotor indicates that it is well suited for power storage.

Two motor/generator units convert the electrical energy from the solar arrays into the kinetic energy of the spinning rotor, and back to electrical energy. Due, in part, to the samarium-cobalt magnets used, the typical efficiency of these units is around 97%. The rotors of these motor/generator units are press fit into the titanium wheel shafts and secured with titanium shaft plugs. These titanium shaft plugs are welded to the titanium wheel, and support the spin bearing and lubrication systems.

Single 204H angular contact ball bearings support the rotor at each end, one bearing is fixed to the inner gimbal, the other floats. In order to improve the high temperature reliability of the bearings and extend their fatigue life, M50 tool steel is specified as the bearing material.

Each bearing has its own lubrication system consisting of a centrifugal oiler, slinger and waste oil retainer. A synthetic hydrocarbon based oil is used as the lubricating agent.

Preloading the bearings is accomplished using a long travel helical spring and a preload adjustment screw. With this arrangement, a preload of 245 N (55 lbs.) would be necessary
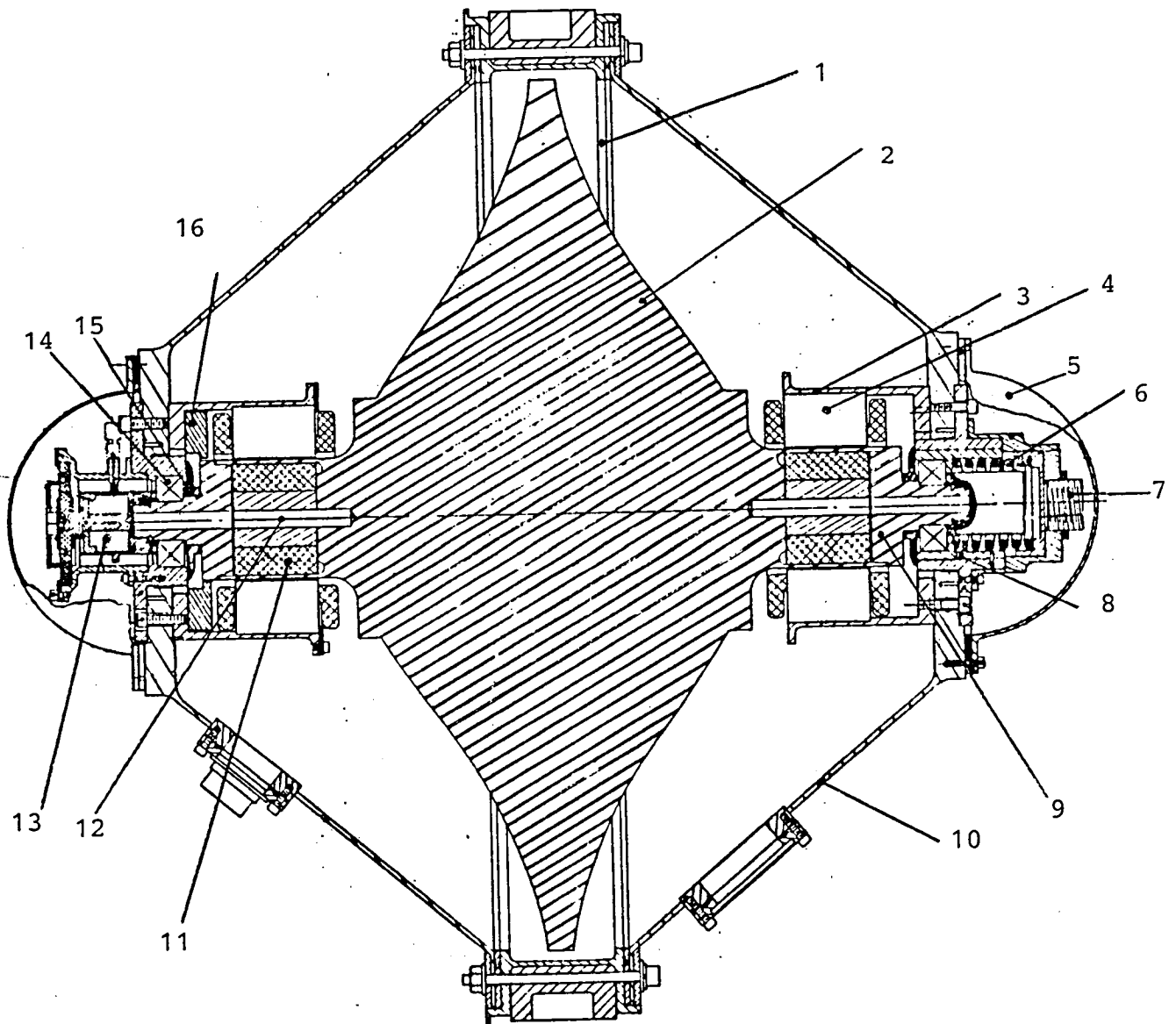
1. Inner Gimbal Ring
2. Rotor
3. Motor/Generator Housing
4. Motor/Generator Stator
5. End Cap
6. Preload Spring
7. Preload Screw
8. Bearing Housing
9. Shaft Plug
10. Inner Gimbal Housing Covers
11. Motor/Generator Rotor
12. Heat Pipe
13. Centrifugal Oiler
14. Spin Bearing
15. Slinger
16. Waste Lubricant Resevoir

Figure 1.   IPACS Inner Gimbal Assembly   (IGA)

for spin axis vertical gimballing operation, on earth. This preload value is required to prevent the unloaded bearing from separating and thereby going unstable.

The inner gimbal assembly is a three piece unit incorporating a central gimbal ring and two stressed skin conical housings. The rotating assembly is supported at the ends of the conical housings. These housings are bolted to the central gimbal ring which provides attachment pads for the gimbal pivots.

2.2 External Gimbal Assembly

The external gimballing assembly incorporates two torque module assemblies (TMA's), two sensor module assemblies (SMA's), an outer gimbal and a mounting ring (see Figure 2).

The TMA's each contain a brushless 2 phase permanent magnet torquer and redundant 16 speed resolvers. Since the required output torque of 27 Nm (20 ft.lbs.) is so low, the torquer motor directly drives the gimbal. The resolvers act as position transducers for the torquer and provide rate feedback information to the gimbal control loop. Electrical power and information is transferred across the interfaces through rotating transformers.

The SMA's contain redundant resolvers for gimbal position sensing and rotary transformers to carry electrical information out to the electronic control systems.

The outer gimbal and mounting ring structures are cast in A356 aluminum. The modified octagonal shapes simplify the mounting of the electronic boxes while providing high stiffness and low weight.

4

SMA

TMA

IGA

Outer Gimbal

Mounting Ring

Figure 2.   IPACS Layout

3.0 Mechanical Analyses

Structural and operational analyses were performed on all of the major IGA components: rotor, spin bearings, lubrication s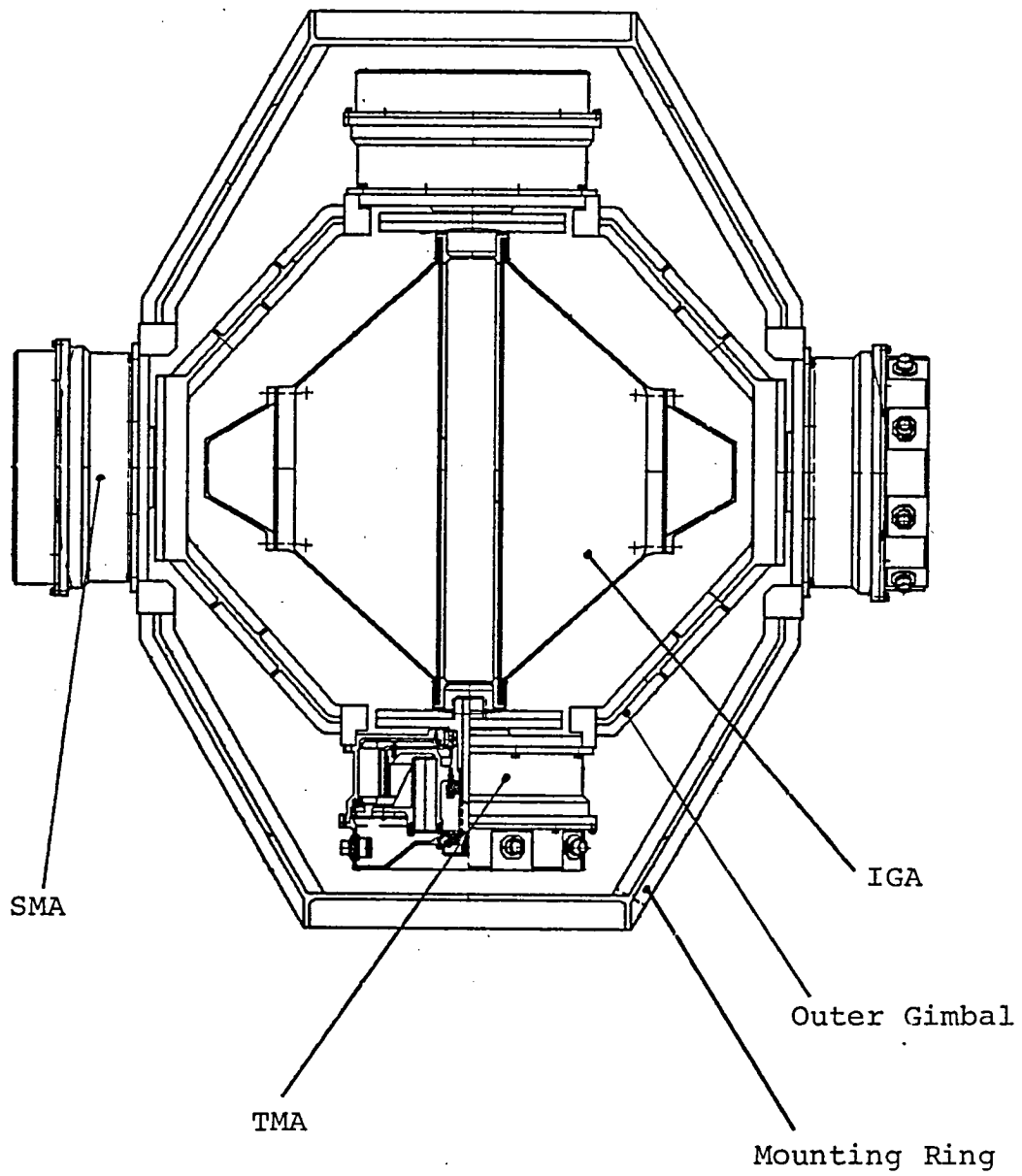ystems, preload mechanism, and inner gimbal. Analyses were also performed on conceptual designs for the outer gimbal and mounting ring structures. Detailed summaries of these efforts are presented in the following sections.

3.1.0 Rotor Analysis

The results of the stress analysis performed on the titanium IPACS rotor are presented in the following sections. The finite element model used in the analysis is described and the analytical results for centrifugal, launch, gimballing and burst loading conditions are presented. Stiffnesses and natural frequencies for the rotor are also given.

3.1.1 Rotor Material

The rotor is machined from a forging of 6Al-4V titanium. This alloy has a very high strength to density ratio making it an efficient flywheel material. The larger the strength to density ratio is, the greater the amount of power that can be stored in a flywheel of a given weight. Physical and mechanical properties of this alloy are presented in Table I.

Table I. Rotor Material Data

Material = Titanium Alloy Ti-6Al-4V
Ultimate Strength (293° K)=896 MPa (68° F=130 ksi)
Ultimate Strength (344° K)=834 MPa (160° F=121 ksi)
Yield Strength (293° K)=827 MPa (68° F=120 ksi)
Yield Strength (344° K)=751 MPa (160° F=109 ksi)
Poisson's Ratio = 0.31
Modulus of Elasticity = 1.10×10^5 MPa (16.0×10^6 psi)
Density = 4430 kg/m^3 (0.16 lbs./in^3)
Fracture Toughness = 76.9 MPa.m$^{0.5}$ (70 ksi.in$^{0.5}$)

There is a significant reduction in strength as the temperature increases from room temperature (293° K or 68° F) to 344° K (160° F). This is important because the heat pipes in the rotor conduct heat away from the spin bearings and motor/generator units and into the body of the rotor. At an operating speed of 35000 rpm, analyses predict

temperatures up to 344° K (160° F) at the center of the rotor (see Reference 1 and Thermal Analysis Section). For this reason, stress evaluations for the rotor during operation must be compared with the lower strengths.

3.1.2 Rotor Model

A finite element model of the rotor was constructed using a finite element modelling program, then analyzed with the computer analysis program, NASTRAN. Data describing the finite element model are given in Table II.

Table II. Rotor Model Data

Nodes = 84600
Elements = 37584
Inertia = 0.789 kg.m^2 (0.582 ft.lbs.sec^2)
Angular Momentum @ 17500 rpm = 1450 N.m.sec
(1070 ft.lbs.sec)
Weight = 56.2 kg (124 lbs.)
Radius = 0.2271 m (8.9428 in.)
Length = 0.4229 m (16.65 in.)

A five degree wedge of the rotor was modeled with 1175 nodes and 522 solid hexahedral elements (see Figure 3). This model is sufficient for analysis of those loading conditions that are symmetrical about the spin axis, such as rotation and axially directed launch loads. For the more complex nonsymmetrical loading conditions, cyclic symmetry is utilized to produce a complete 360 degree model of the rotor with 84600 nodes and 37584 elements. The model is titanium except for the iron and samarium cobalt motor/generator rotors. Those elements that model the motor/generator rotors have higher densities to conform with the weights reported in Reference 1. Constraints on the rotor model are consistent with the reaction of the actual spin bearing system. One end of the model is "fixed" at the bearing location in that no radial or axial movement is allowed. The other end is "floated" by constraining only radial motion and permitting axial motion.

The rotor shape is derived from a "constant stress" criterion that purports to equalize the centrifugal stress at any given radius from the center of the rotor. As stated in Reference 2, the equation controlling the contours would be:

$$Z = ce^{-(\rho \omega^2 r^2 /2\sigma)}$$
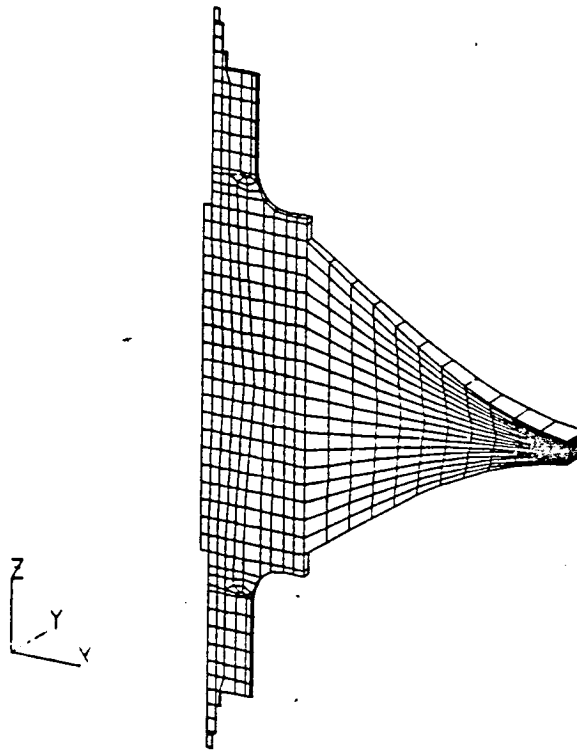
Figure 3. Finite Element Model of Rotor

Substituting in half the tip thickness Z=0.01298 m (0.511 inch) at the tip radius r=0.2271 m (8.9428 inches) and half the rotor thickness Z=0.1121 m (4.4128 inch) at r=0.0 m, and inserting 3665 rad/sec for ω and 4430 kg/m^3 (4.141x10^{-4} lbs.sec^2/in^4) as ρ gives 536.2 MPa (78060 psi) for σ and 0.1121 m (4.4128 in.) for c.

Therefore, the equation for one quarter of the rotor contour is:

$$Z=(0.1121)(e)^{-(4430)(3665)^2(r)^2/(2)(5.362x10^8)}$$

for values of r from 0.0 to 0.2271.

A contour plot of the Von Mises effective stress for the rotor is shown in Figure 4 of the Centrifugal Stress Section. Note that near the middle of the rotor, constant stress contours form nearly spherical shells about the center. In this way, strain energy per unit volume is maximized, and with it, the power storage density of the rotor.

8

3.1.3 Loading Condition

Stress analysis was performed on the rotor in both launch and operational environments. The two launch environments analyzed were 20 g's axial acceleration and 20 g's lateral acceleration. This 20 g launch environment is conservatively high for Space Transportation System (STS) launches. Operational stresses were determined at speeds of 24000, 30800 and 35000 rpm with a gimballing torque of 27 Nm (20 ft.lbs.).

3.1.4 Centrifugal Stress Analysis

The IPACS rotor is designed to cycle up and down between 17500 rpm and 35000 rpm. When the spacecraft is in the sun lit portion of its orbit, electrical energy is stored as kinetic energy by driving the rotor up to 35000 rpm. Later on, during the night time of the orbit, the stored energy is recovered through the generators as the rotor spins down to 17500 rpm. Since a complete orbit occurs every 90 minutes, there would be about 33300 storage cycles over the design lifetime of 5.7 years. This extensive cyclic history is important as it will constrain the IPACS maximum operating speed to 30800 rpm.

To understand fully this limitation, a more thorough examination of the design is required. As the rotor spins up to 35000 rpm, metal in the center of the rotor becomes stressed beyond its yield strength. When this occurs, the material undergoes a transition from elastic to plastic behavior.

Elastic behavior is recognized by the linear relationship between applied stress and the resulting strain or deformation. The stress is absorbed as strain energy when the material deforms, but no permanent deformation exists. Upon removal of the stress, the material returns to its original shape. If the yield strength of the material is surpassed, plastic behavior ensues. While the material continues to deform in reaction to the increased stress, this additional deformation is permanent.

When the IPACS rotor is spun at 35000 rpm, a center region of the rotor is stressed into plastic behavior and permanent strain or deformation occurs. The rest of the rotor is not stressed as high and remains elastic. If the rotor is stopped, the elastic shell will shrink around the

plastically deformed center region and compress it back into shape. Therefore, at zero speed there is a stress distribution inside the rotor. The elastic shell is under tension and the yielded region at the center is under compression. Because of this internal prestressing, the rotor may now be spun up to 35000 rpm and no part of the rotor will be stressed beyond the elastic limit. Plastic deformation would occur only the first time the rotor was driven to 35000 rpm. There after, the prestressed nature of the rotor would allow operation up to 35000 rpm while keeping the maximum stresses entirely within the elastic range of the material.

Rockwell believed that the initial plastic deformation required to prestress the rotor would have little effect on the overall operation of the system. However, Bendix feels this one time plastic deformation would render this elasto-plastic prestressing concept unworkable.

The basic flaw in this concept is the increased probability of a brittle fracture type of failure. When the center of the rotor deforms plastically, micro flaws and voids are formed in the material. During the normal operation of the wheel, but after the initial prestressing run up, the stress at the center of the rotor will range from 21 MPa to 751 MPa (3 ksi to 109 ksi) as the rotor is cycled from 17500 rpm to 35000 rpm. This large alternating stress would cause the micro flaws to propagate until brittle fracture occurred. This is why the extensive cyclic environment of the IPACS is so important. It is this action upon the yielded center that would induce premature failure.

However, by reducing the top speed of the rotor so that no plasticity occurs, this problem may be resolved. If the maximum speed of the rotor was reduced to 30800 rpm at a worst case operating temperature of 344° K (160° F), then the peak stress would be equal to the yield strength of the titanium (751 MPa or 109 ksi). As the rotor would now be operating in a purely elastic stress range, there would be no plastic deformation. Consequently, no micro flaws would be formed to act as nuclei for failure causing cracks.

Factors and margins of safety against the yield and ultimate strengths of the titanium are presented in Table III. Note that the maximum stress at 35000 rpm is only 3% higher than at 30800 rpm. This is due to the fact that at speeds above 30800 rpm the rotor behaves plastically and the stress increases nonlinearly.

(0-20 ksi)   0-138 MPa

(20-40 ksi)   138-276 MPa

(40-60 ksi)   276-413 MPa

(60-80 ksi)   413-551 MPa

(80-100 ksi)   551-689 MPa

(100-120 ksi)   689-827 MPa
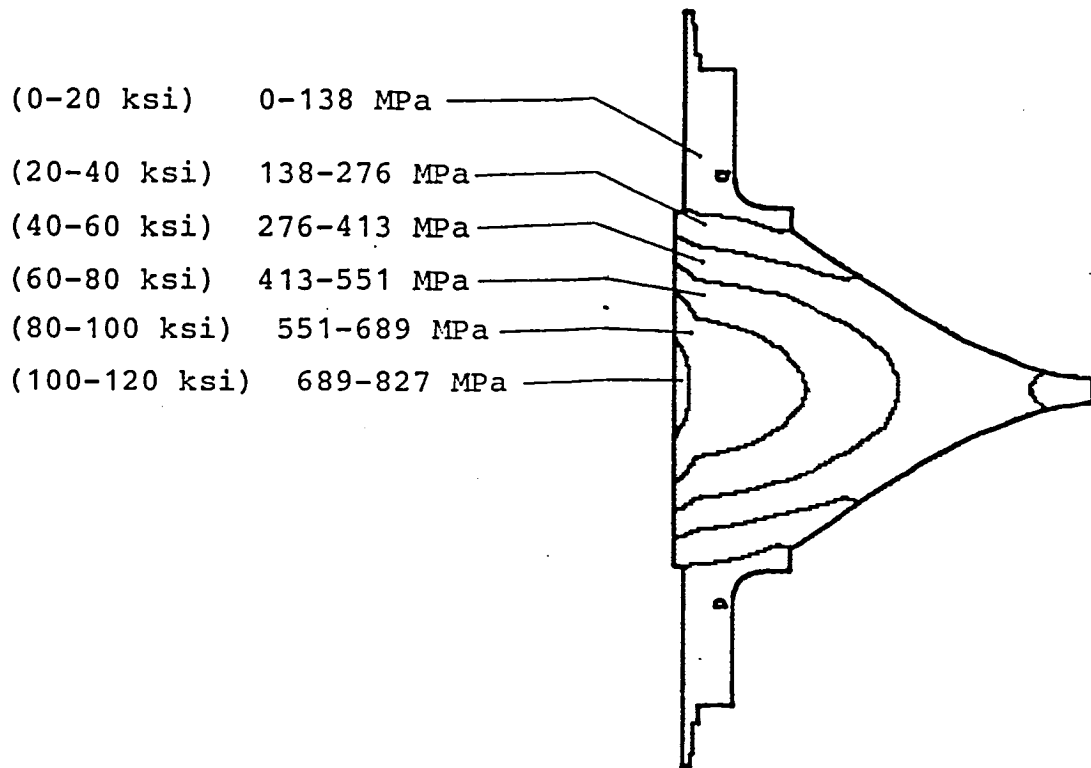
Figure 4. Centrifugal Stress in the Rotor at 30800 RPM and 344° K (160° F)

At 30800 rpm, the factor of safety with respect to yield is 1.0 (F.S.=Y.S./STRESS=751 MPa/751 MPa), and the margin of safety with respect to yield is 0.0 (M.S.=F.S.-1.0). Although these factors would be larger with respect to the ultimate strength of the titanium and higher still with respect to the burst speed of the rotor, they would still be below what is currently acceptable for manned space flights. An IPACS at 30800 rpm is technically feasible but could not be qualified as flight hardware. Bendix designed and built the CMGs for the manned Apollo Telescope Mount (ATM) vehicle and was instructed by NASA/MSFC to limit rotor stresses to one third of the rotor material's strength. This factor of safety of 3 is a typical design limitation for most, if not all of the CMGs and reaction wheels used for vehicle control to date. For this reason, the maximum operating speed of this rotor should be kept down to around 24000 rpm.

Table III. Factors and Margins of Safety for the Rotor

Speed	Stress	Factors		Margins	
		Yield	Ultimate	Yield	Ultimate
35000 rpm	+772 Mpa	0.97	1.07	-0.03	0.07
	+112 ksi				
30800 rpm	751 MPa	1.00	1.10	0.00	0.10
	109 ksi				
24000 rpm	455 Mpa	1.65	1.83	0.65	0.83
	66 ksi				

To preserve the 75% depth of energy discharge, the minimum speed of the rotor should be reduced to 12000 rpm. 50% of the top speed equates to 25% of the top kinetic energy and hence the 75% discharge over the 50% speed variation.

There is a considerable loss of power storage capability when limiting the top speed of the rotor to 24000 rpm. Since energy storage is proportional to the square of the angular velocity, the top speed derating reduces the rotor's power capability from 2200 watts to 1040 watts.

While some of this loss may be regained by using materials with higher strength to density ratios, the primary constraint for this flywheel is at what factor of safety it may operate. For any given rotor operating in the elastic domain, power storage capability is inversely proportional to the factor of safety. This relationship for the IPACS rotor is depicted in Figure 5.

Since the rotor configuration and material are nearly optimal in this application, the only way to substantially increase the power storage capability is either to reduce the safety factor by increasing the top speed, or by altering the centrifugal stress distribution by prestressing. As was described earlier in this section, an internal prestressing approach was used on the IPACS rotor. Were it not for the uncertain reaction of the plastic material to crack growth, this approach would be acceptable. Clearly, further analysis and experimentation on the fracture toughness and crack propagation characteristics of yielded metals would be invaluable in extending the power storage capabilities of flywheels. However, until such time that this reaction is known with some amount of confidence, it is not considered wise to utilize it.
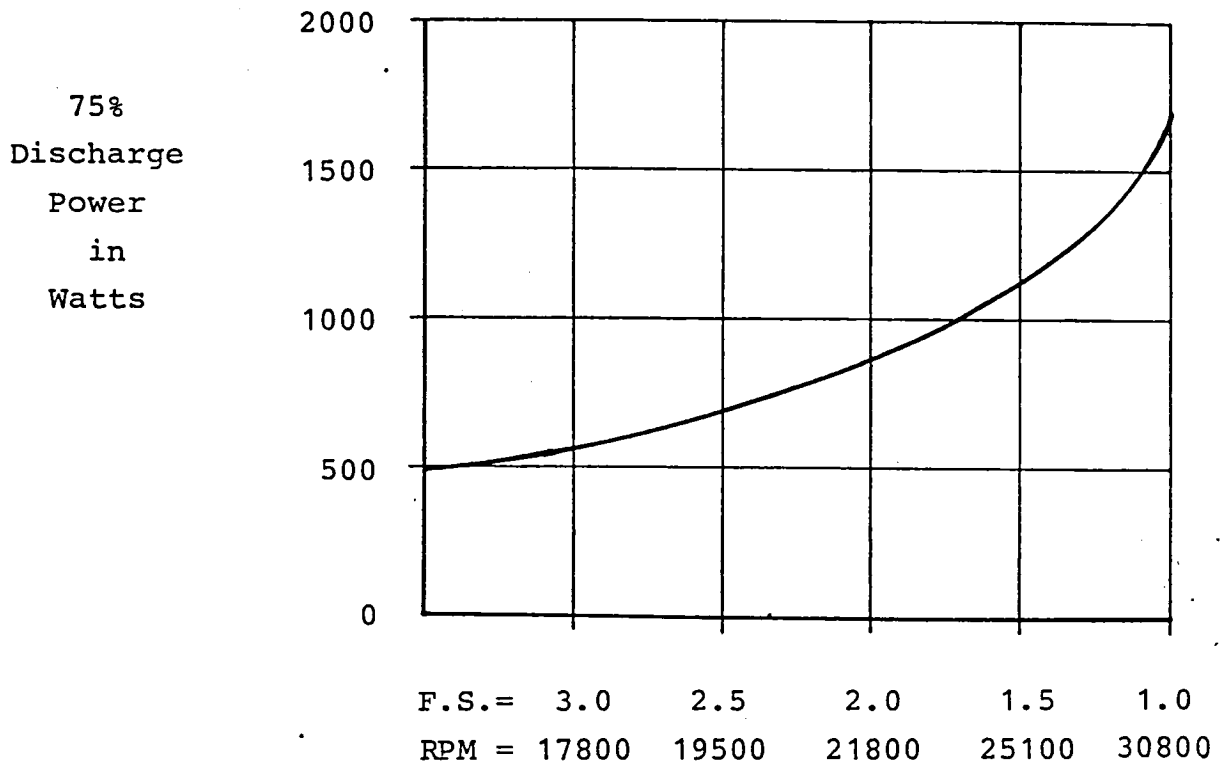
Figure 5.   IPACS Power Storage Capability versus Factor of
Safety on Yield Strength (and Maximum Rotor Speed)

3.1.5 Launch and Gimballing Stress Analyses

The rotor was evaluated for stresses induced by axial and
lateral launch accelerations.   Maximum stresses in both
cases are concentrated in the bearing support areas and are
quite small.   A 20 g launch acceleration directed axially
produces a maximum stress of 58.6 MPa (8.5 ksi).   The same
20 g's directed laterally results in a stress of less than
6.9 MPa (1 ksi).

The gimballing rate necessary to achieve the required 27 Nm
(20 ft.lbs) of precession torque is 0.019 radians per second
at a rotor speed of 17500 rpm.   This is a very benign
environment and results in a maximum stress far below 6.9
MPa (1 ksi).

13

3.1.6 Stiffnesses and Natural Frequencies

Stiffness calculations are based on "rigid" bearing assumptions.

Axial Stiffness = 6.46×10^8 N/m   (3.69×10^6 lbs./in.)
Lateral Stiffness = 5.74×10^9 N/m   (3.28×10^7 lbs./in.)

The natural frequencies computed from these stiffnesses correlate extremely well with the natural frequencies determined in the modal analysis, as shown in Table IV.

Table IV.   Rotor Natural Frequencies

Mode	Frequency from Stiffness model wt = 552 N (124 lbs.)	Frequency from Modal Analysis
Axial Mode	540 Hz.	554 Hz.
Lateral Mode	1609 Hz.	1613 Hz.

3.1.7 Burst Speed

The burst speed of a rotor is essentially a problem of stability or dynamic equilibrium. There are two mechanisms by which instability -and therefore burst- may occur: brittle fracture and ductile fracture.

Brittle fracture may occur at stress levels far below the yield strength of the material. The presence of a flaw in the material can cause a large increase in stress at that point, depending upon the size, type and configuration of the flaw and its orientation in the stress field. If this stress magnification is high enough, the flaw will begin growing. In some cases this growth is rapid, unstable and self propagating, and quickly leads to brittle fracture failure.

This failure mode can be avoided by careful selection of fracture tough materials and attention to inspection and quality control procedures. Because brittle fracture requires a flaw as a starting point, any steps that can be taken to minimize flaws in the structure will also minimize the possibility of this type of failure occurring.

The second mechanism through which burst can occur is ductile fracture or plastic deformation. Again, the circumstances determining failure vary greatly depending

upon the structure. For dual and single webbed rotors, burst occurs at stress levels very near the yield strength of the material. The highest stressed area in a single webbed rotor is usually at the thin sectioned web out near the rim. The web supports the rim and yielding at this point results in loss of control of the rim. In most dual web rotors, peak centrifugal stresses occur in the rim and yielding at this point results in loss of control of the rim. Either way, the instability caused by the loss of control quickly leads to the destruction of the rotor.

For solid rotors like that used in the IPACS IGA, burst speed is not as sensitive to the onset of plasticity, but rather depends upon the volume of the material that has yielded. The highest stressed area in a solid rotor is at the center. But when the center yields, there is no substantial plastic deformation because of the large amount of elastic material surrounding the plastic zone. This elastic shell acts as a containment vessel to control the plastic center. As the rotor speed increases, the plastic zone expands till the elastic shell of the rotor can no longer control it, and burst occurs.

Original analysis, by Rockwell, (Reference 1) predicted a burst speed of 44300 rpm. This speed was calculated using an inhouse experimentally derived formula based on the average tangential stress in the flywheel, the ultimate tensile strength of the material, and a burst factor derived from the elongation property of the material.

Two finite element analyses were performed in this current Bendix effort to substantiate the 44300 rpm burst speed prediction. A nonlinear material analysis was performed on the rotor model to determine at what speed the wheel would become unstable and explode. The stress vs. strain curve shown in Figure 6 was input into NASTRAN and the rotor speed incremented in 1000 rpm steps till burst was reached. At 38000 rpm the analysis converged to a stable equilibrium while at 39000 rpm the situation became unstable and the analysis diverged. This instability and the corresponding inability to determine a stable dynamic equilibrium at this speed would indicate that the burst speed of the rotor is no higher than 39000 rpm.

In order to verify this conclusion a similar but not as sophisticated procedure was used. The wheel was analyzed at 38000 rpm with a linear elastic analysis. Those elements in the finite element model that were at the highest stress (above the ultimate strength) were altered so that they had a very low modulus of elasticity. Then the model was
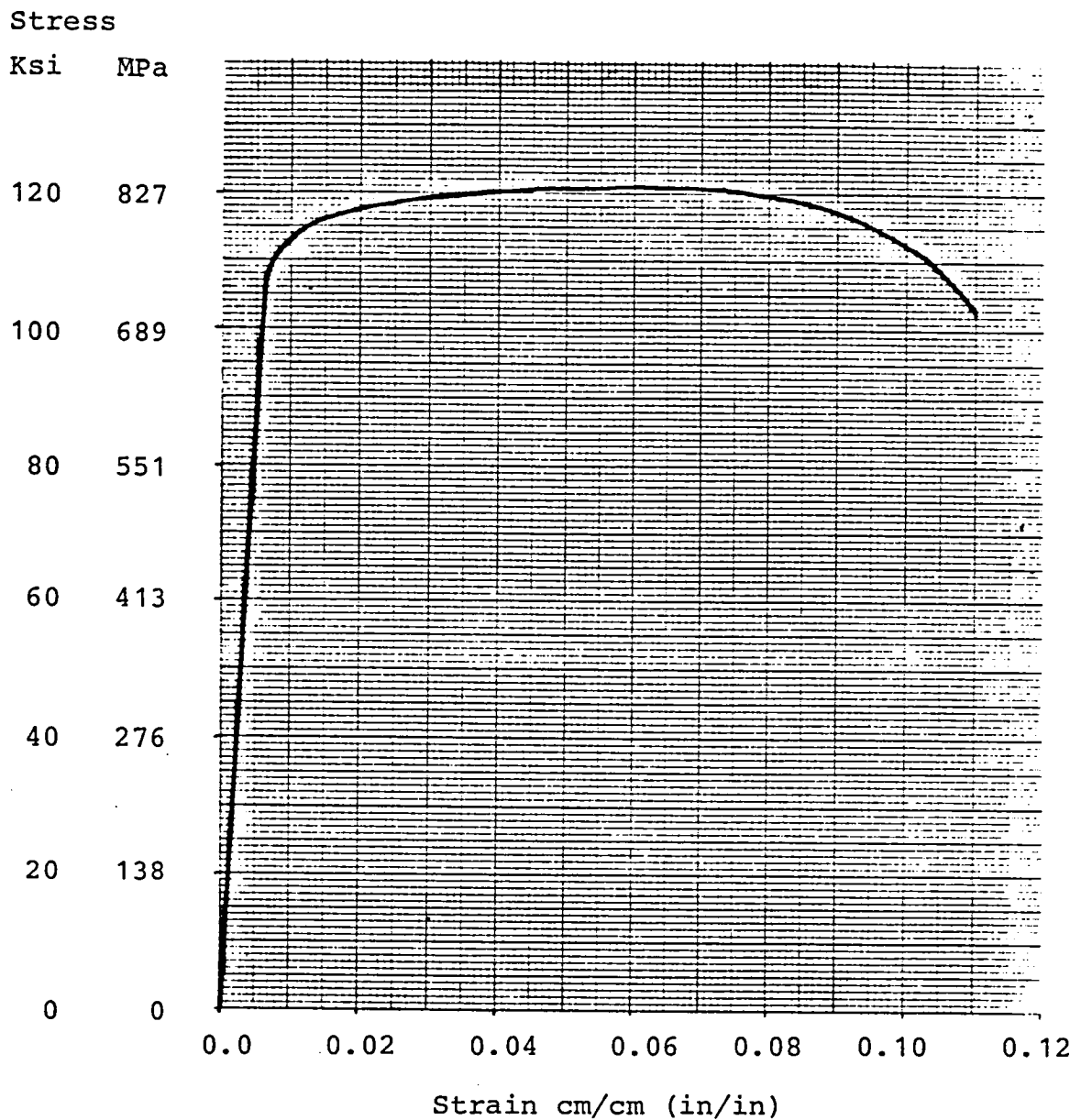
Stress

Ksi   MPa

Figure 6.   Stress versus Strain for Titanium 6Al-4V at
            344° K (160° F).

reanalyzed at 38000 rpm and more elements altered.   This
procedure would be continued in an iterative fashion until
either of two conditions occurred: equilibrium, with all

material below the ultimate strength of titanium; or instability, where altering the elements would result in abrupt and large increases in the stress distribution. It was this latter condition that finally occurred. Throughout a dozen iterations the stress distribution had steadily been dropping. On the 13th iteration the distribution changed radically and large areas of the surface became overstressed beyond the ultimate strength of the titanium. This abrupt instability supports the conclusion reached through the nonlinear analysis that the burst speed of the rotor is between 38000 and 39000 rpm. This second analysis effort assumes the material that has yielded has no inherent strength but is retained by the outer shell of the rotor similar to a fluid in a container.

It is important to realize that these calculations utilize the worst case strengths at 344° K (160° F) as published in Reference 3, while the actual forging strengths of this rotor are almost certain to be higher. A review of the material certifications of many of the Bendix rotor forgings indicate that actual material strengths average from 10% to 20% higher than the minimum requirements. If this situation existed with the IPACS rotor forging it would easily extend the predicted burst speed into the 42000 rpm to 43000 rpm range. This condition is supported by the fact that the IPACS rotor has been tested up to 38500 rpm without failing. Consequently, a considerable gain in system efficiency could be had if the performance limits for each rotor were based on test results taken from samples from each rotor forging blank. As an example, a 20% increase in material strength would allow a 9.5% increase in the maximum rotor speed and a 20% increase in the rotor's storage power.

3.2.0 Spin Bearing Analysis

The IPACS spin bearing system consists of two 204H angular contact ball bearings, two centrifugal oilers and a spring controlled preload mechanism (see Figure 7). The system was analyzed in four separate areas: lubrication, preloading, drag torque and reliability.

3.2.1 Lubrication

Lubrication of the spin bearings depends upon a centrifugal oiler system. Rotation of the oil reservoirs at the wheel speed produces a pressure that pushes the oil through the flow restrictors and into the spin bearings. Slingers capture the used oil as it drains from the spin bearing and directs it to a waste oil retainer.
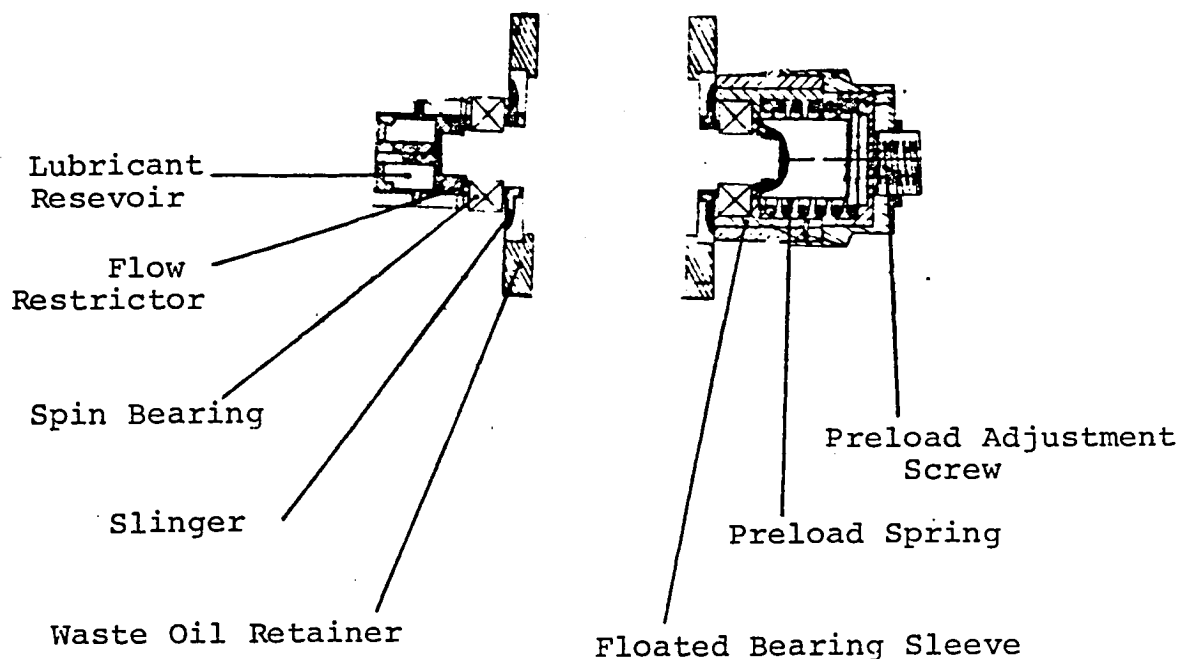
Figure 7.   IPACS Spin Bearing System

The lubricant is a synthesized hydrocarbon based oil
(Mobil's SHC-630) which works well in the high speed, high
temperature environment of the IPACS.   Lubricant data for
the oil are presented in Table V.   A plot of viscosity
versus temperature is shown in Figure 8.

Table V.   IPACS Spin Bearing Lubricant Data

Lubricant	= Mobil SHC-630 Oil
Type	= Synthesized Hydrocarbon
Pressure Viscosity Coefficient	= 3.54×10^{-2} MPa^{-1}
	= 2.44×10^{-4} psi^{-1}
Thermal Conductivity	= 0.104 W/(m.$^{\circ}$K)
	= 6.0×10^{-2} BTU/(ft.$^{\circ}$F.hr)

The concerns regarding lubrication were threefold: 1) will
there be enough oil flow at 17500 rpm and room temperature,
2) will there be too much oil flow at 35000 rpm at 366° K
(200° F), and 3) will there be a sufficient supply of oil
available at the end of 5 years.

18

Figure 8.   Viscosity versus Temperature for Spin Bearing
            Lubricant.

Assuming continuous operation at 35000 rpm and 366° K
(200° F) with an initial charge of 7.25 grams of oil, the

flow at the end of 5 years drops to 0.051 mg/hr from an initial 0.160 mg/hr and the amount of oil remaining is 2.38 grams.

The room temperature flow at 17500 rpm would be 0.0031 mg/hr at the 5 year point versus an initial flow rate of 0.0097 mg/hr. All of these values appear satisfactory from an analytical standpoint. Concern exists, however, relative to hardware performance under these various flow rate conditions. E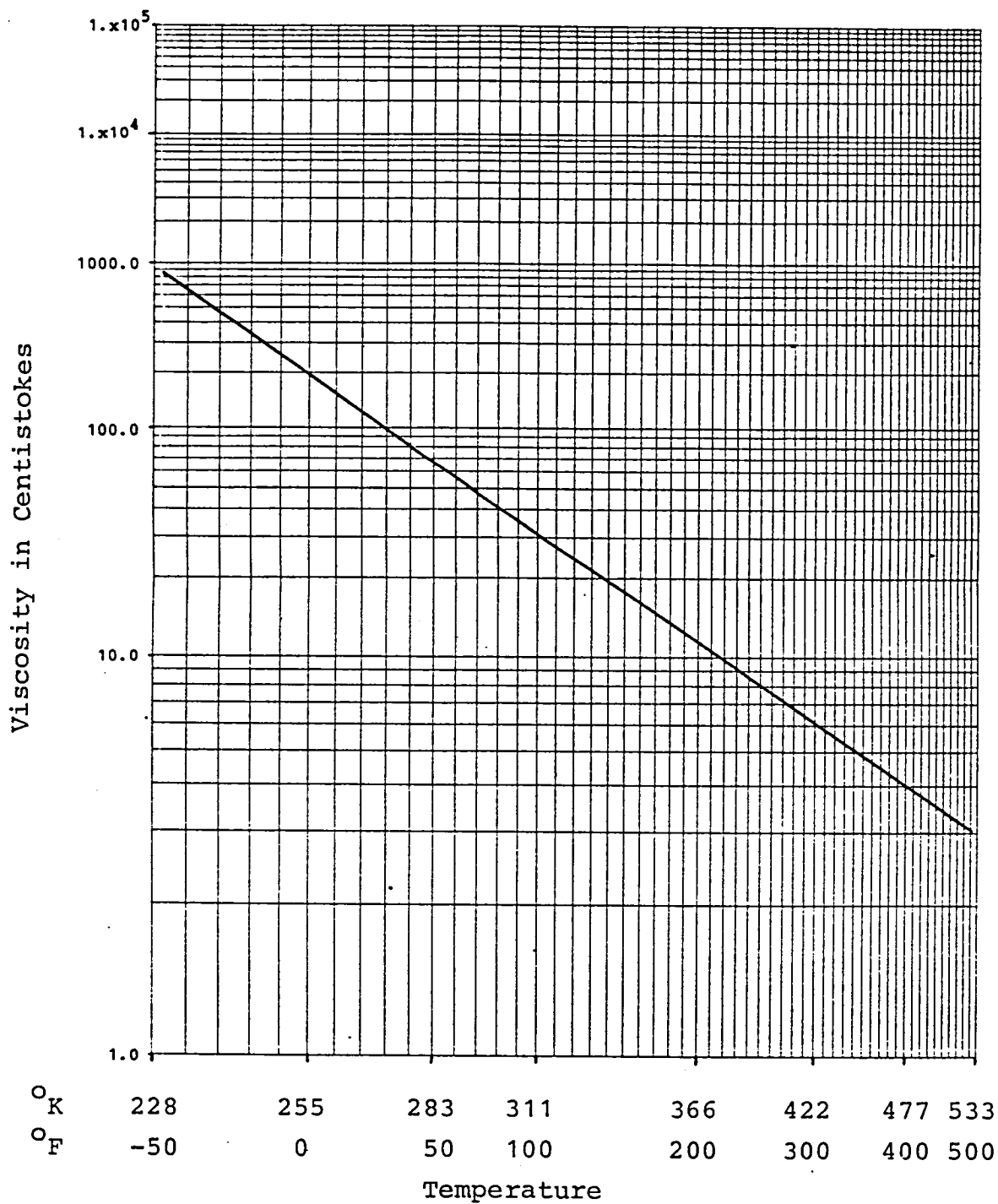xtensive flow rate testing and life testing are essential in establishing performance and a flow rate testing program should be developed to evaluate drag torque on the spin bearings.

3.2.2 Preloading

Currently, the floated bearing utilizes a helical spring with an adjusting screw to change the preload force value. The fixed side incorporates interference fits at both the inner and outer races. The preload spring is presently set at 67 N (15 lbs.) force with a recommended value of 134 N (30 lbs.) for vertical or gimballing operation.

In a worst case condition of spin axis (SA) vertical, on earth testing with the bearings at 366° K (200° F), the fixed bearing interference fits nearly go to zero:

$$\delta = \Delta\alpha \ \Delta T \ d$$
$$\delta = (2.6 \times 10^{-6} \ cm/cm/^O K)(72^O \ K)(2.00 \ cm)$$
$$\delta = 0.00037 \ cm$$

Interference fit = 0.00050 - 0.00037 = 0.00013 cm

where: δ is the diametral difference, in centimeters caused by the thermal expansion.

$\Delta\alpha$ is the difference in thermal expansion coefficients between titanium (8.6×10^{-6} cm/cm/^{O}K) and M50 tool steel (11.2×10^{-6} cm/cm/^{O}K)

ΔT is the temperature change from assembly (294° K or 70° F) to operating temperature (366° K or 200° F).

d is the bore of the bearing = 2.00 cm

Because the interference fits provide little, if any, preloading during operation of the IPACS, all of the preload force must be generated through the spring mechanism. In a spin axis (SA) horizontal configuration both bearings are preloaded equally and are compressed the same amount. When

the unit is moved to a SA vertical configuration, the lower bearing compresses further, for it now supports the entire weight of the wheel. As the lower bearing compresses due to the wheel weight, the upper bearing expands by the same amount since the two bearings are tied together through the rotor. If the top bearing expands more than it was originally compressed during preloading, the bearing will separate, become unstable and fail. As long as the top bearing does not expand more than it was originally compressed, there will always be some residual compression, and therefore preload, in the bearing which will allow it to run in a stable condition. The preload required in this system is about 245 N (55 lbs):

    Bearing Compression Due to Preloading:
        245 N = 0.0173 mm
        55 lbs = 683 microinches

    Force on Lower Bearing During SA Vertical Operation:
        = Rotating Assembly Weight + Pumping Force + Preload
        = 57.6 kg + 22 N + 245 N = 832 N
        = 127 lbs + 5 lbs + 55 lbs = 187 lbs

    Total Bearing Compression in Lower Bearing During SA Vertical Operation:
        832 N = 0.0345 mm
        187 lbs = 1360 microinches

    Lower Bearing Compression due to SA Vertical Operation is equal to the Upper Bearing Expansion and is equal to:
        0.0345 mm - 0.0173 mm = 0.0172 mm
        1360 microinches - 683 microinches = 677 microinches

Since the bearing compression due to preloading (0.0173 mm) is greater than the bearing expansion that occurs in SA vertical operation (0.0172 mm), the top bearing will not unload and the preload value of 245 N (55 lbs) is considered adequate.

This preload value of 245 N (55 lbs.) is considerably higher than the 133 N (30 lbs.) that was originally expected, and higher drag torques, hotter bearing temperatures and greater power losses will occur. For these reasons, it would be advantageous to redesign the preloading mechanism to use bellville washers on each end. This approach would allow a preload as low as 67 N (15 lbs.) for gimballing operation, thus reducing drag torque while increasing reliability and efficiency. This type of preloading will be investigated during Phase II activities.

3.2.3 Drag Torque

Drag torque on a bearing is the sum total of viscous drag plus drag from radial loading and drag from thrust loading. Viscous drag at 35000 rpm for 2 bearings is calculated to be:

$$T_V = 2 \times 0.05 \times (7.98 \times 10^{-2} \text{ Nm}) = 7.98 \times 10^{-3} \text{ Nm}$$

where:
T_V is the viscous drag.
2 is the number of bearings.
0.05 is a Bendix conversion assuming KG-80 oil and ABEC 9 bearings.
7.98×10^{-2} Nm is Barden's bearing torque value.

For the SA horizontal, on earth operation and 67 N (15 lbs.) preload, there is a radial load of 282 N (63.5 lbs.) per bearing from the wheel weight and a preload thrust load of 67 N (15 lbs.) per bearing. The drag torque due to radial loads from Figure 9 is:

$$T_R = 2.47 \times 10^{-3} \text{ Nm} \times 2 = 4.94 \times 10^{-3} \text{ Nm}$$

And the drag torque due to the thrust loading would be:

$$T_T = 9.89 \times 10^{-4} \text{ Nm} \times 2 = 1.98 \times 10^{-3} \text{ Nm}$$

Therefore, the total drag would be:

$$T_{TOTAL} = (7.98 + 4.94 + 1.98) \times 10^{-3} \text{ Nm} = 1.49 \times 10^{-2} \text{ Nm}$$

The conversion to watts is:

$$P = \frac{\text{Torque x RPM}}{9.55} = \frac{(1.49 \times 10^{-2})(35000)}{9.55}$$

or P = 54.6 watts versus the 44 watts listed in Reference 1.

The worst case drag torque power is determined at the maximum operating speed of the rotor: 24000 rpm (see Rotor Analysis), on earth operation, SA vertical with the current preloading mechanism at 245 N (55 lbs.) of preload. Drag torque power in this configuration is 88 watts. Redesigning the preload mechanism to include bellville washers would lower the preload to 67 N (15 lbs.), and reduce the drag torque power 25% to 66 watts. The drag torque differential

Load

lbs.	N.
400	1780
300	1335
200	890
100	445
50	222
25	111
10	44

Radial

Thrust

0.7   7.0   70

$*10^{-3}$ Nm

0.1   1.0   10

in.oz.
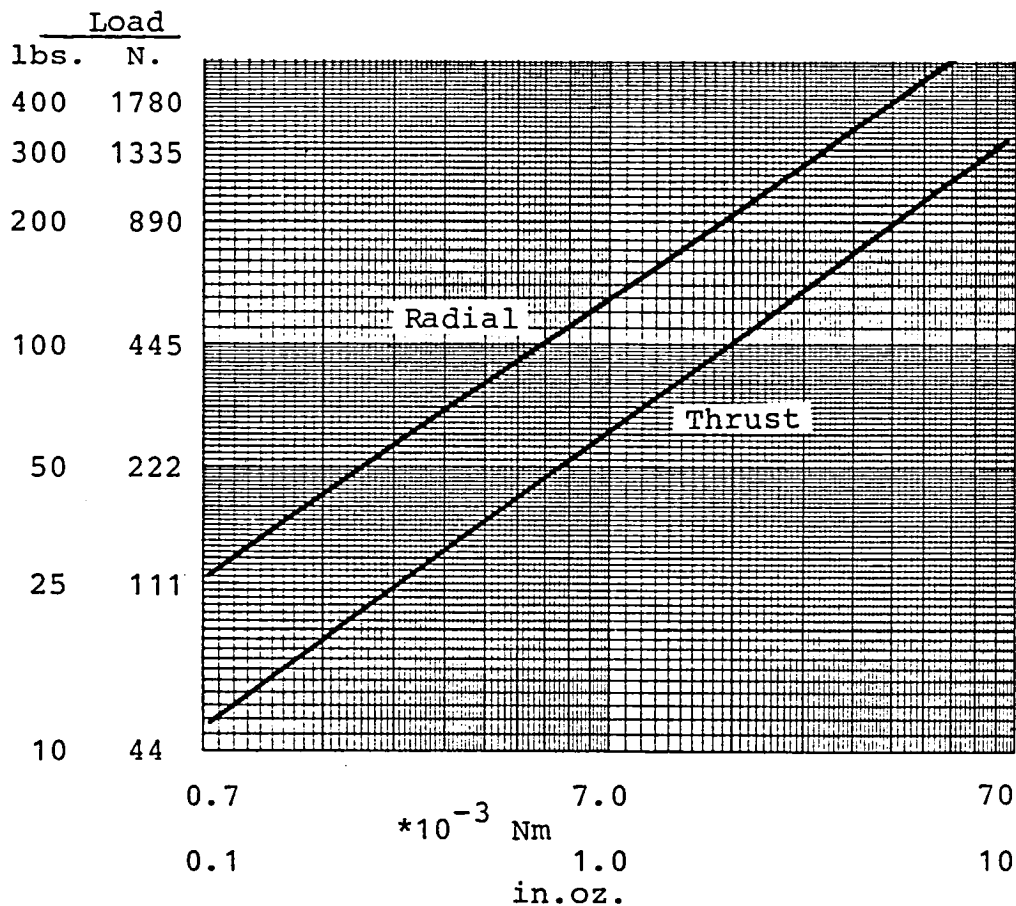
Figure 9. Spin Bearing Drag Torque Data

between the two preloading systems is even more substantial in space with only 10 watts of drag torque power being used at a bearing in the bellville washer system as opposed to 22 watts dissipated through the fixed bearing of the current design, a decrease of 120%!

3.2.4 Reliability

Bearing reliability is determined using the Jone's high speed ball bearing computer program (Reference 2). Input to the program includes the geometry, material and surface finishes of the balls and races of the bearing, influence coefficients for the rotor and inner gimbal, lubricant data, and an extensive loading history encompassing all phases of testing and operation.

Each bearing contains 10 balls, each of which is 7.9375 mm (0.3125 inch) in diameter. Detailed spin bearing geometry data are presented in Table VI.

Table VI. Spin Bearing Geometry Data

Ball Size	=	7.9375 mm	=	0.31250 inch
Number of Balls	=	10		
Outer Race Curvature	=	0.540		
Inner Race Curvature	=	0.520		
Bore	=	20.00 mm	=	0.78740 inch
Outer Race Diameter	=	47.00 mm	=	1.8504 inch
Outer Race Groove Diameter	=	41.75 mm	=	1.6438 inch
Inner Race Groove Diameter	=	25.84 mm	=	1.0175 inch
Outer Race Land Diameter	=	38.86 mm	=	1.53 inch
Inner Race Land Diameter	=	28.70 mm	=	1.13 inch
Width	=	14.00 mm	=	0.55120 inch
Radial Play	=	0.033 mm	=	0.00130 inch
Free Contact Angle	=	15.13 degrees		

M50 tool steel (AMS 6490) is specified as the bearing material, this being a high speed, high temperature metal with enhanced fatigue properties. Refined processing of this material allows a life adjustment factor of 6 to be used in the reliability analysis. Original design specifications indicate surface finishes of 1.524×10^{-4} mm (6 microinches) and 2.54×10^{-5} mm (1 microinch) for the races and balls respectively.

The loading environment for the spin bearings was divided into two phases: an 800 hour earth based testing period and a 10000 hour operational period. The IPACS concept assumed that bearing replacement would occur at 10000 hour maintenance intervals throughout the lifetime of the system. For this reason, spin bearing reliability calculations were performed with respect to this 10800 hour time frame.

A value of 24000 rpm was chosen as a reasonable top speed for the system given the results described in the rotor analysis section. A minimum speed of 17500 rpm was retained to satisfy the angular momentum requirements of the system. Bearing speed was considered the only variable occurring during the operational period so two 5000 hour environments were applied: one at 24000 rpm and the other at 17500 rpm. A 27 Nm (20 ft.lbs.) gimballing torque and a 8.9 N (2 lbs.) rotor unbalance force were applied continuously to both cases.

The 800 hour earth based testing period had to be divided into six different loading cases. Spin bearing loading was initially divided by speed into two subcases: a high speed subcase of 400 hours at 24000 rpm, and a low speed subcase of 400 hours at 17500 rpm. Each subcase was further divided

into two 200 hour periods for spin axis vertical and spin axis horizontal operation. Loading on the bearing system in the spin axis horizontal configuration was applied as a radial load equal to the weight of the rotor and this was distributed equally between the two bearings. However, during spin axis vertical operation one bearing supports the weight of the rotating assembly by itself while the other bearing free wheels with only a slight residual thrust load remaining to prevent it from completely unloading. Since the Jone's program analyzes the spin bearings as a system, it was necessary to further subdivide the 200 hour spin axis vertical load cases into 100 hour subcases so that each bearing would receive identical loading histories. One 100 hour subcase applied the rotor weight in the positive spin axis direction while the other 100 hours applied the weight in the negative spin axis direction. In this way, support of the rotor during spin axis vertical operation is split equally between the two bearings. As was done for the operational loading conditions, a 27 Nm (20 ft.lbs.) gimballing torque and a 8.9 N (2 lbs.) rotor unbalance force were applied continuously during all six testing environments. Clarification of the spin bearing's loading history may be found in Figure 10.

Output from the bearing analysis program is extremely detailed and includes ball deflections, loads, stresses, torques and speeds. Elastohydrodynamic lubrication effects are analyzed and the expected life of the bearing system at some reliability level is computed.

Reliability for the 10800 hours of testing and operation of the spin bearings is predicted to be 99.8%. This improvement over the original IPACS determination of 97.8% is due to the decrease in maximum operating speed from 35000 rpm to 24000 rpm.

M50 tool steel was originally specified in the IPACS design for its increased fatigue life and high temperature stability. However, state of the art material processing will currently produce high purity VIM-VAR 52100 bearing steel with life adjustment factors equal to or greater than the M50 tool steel was 10 years ago. Furthermore, the high temperature stability of the 52100 steel has been extended out to 465° K (375° F), far beyond the worst case temperatures that the bearings will see. For these reasons it would be reasonable to down grade the bearing material specification from the exotic M50 tool steel to the standard refined 52100 bearing steel. The difference in bearing reliability would be insignificant while the cost and lead time reductions would be appreciable.
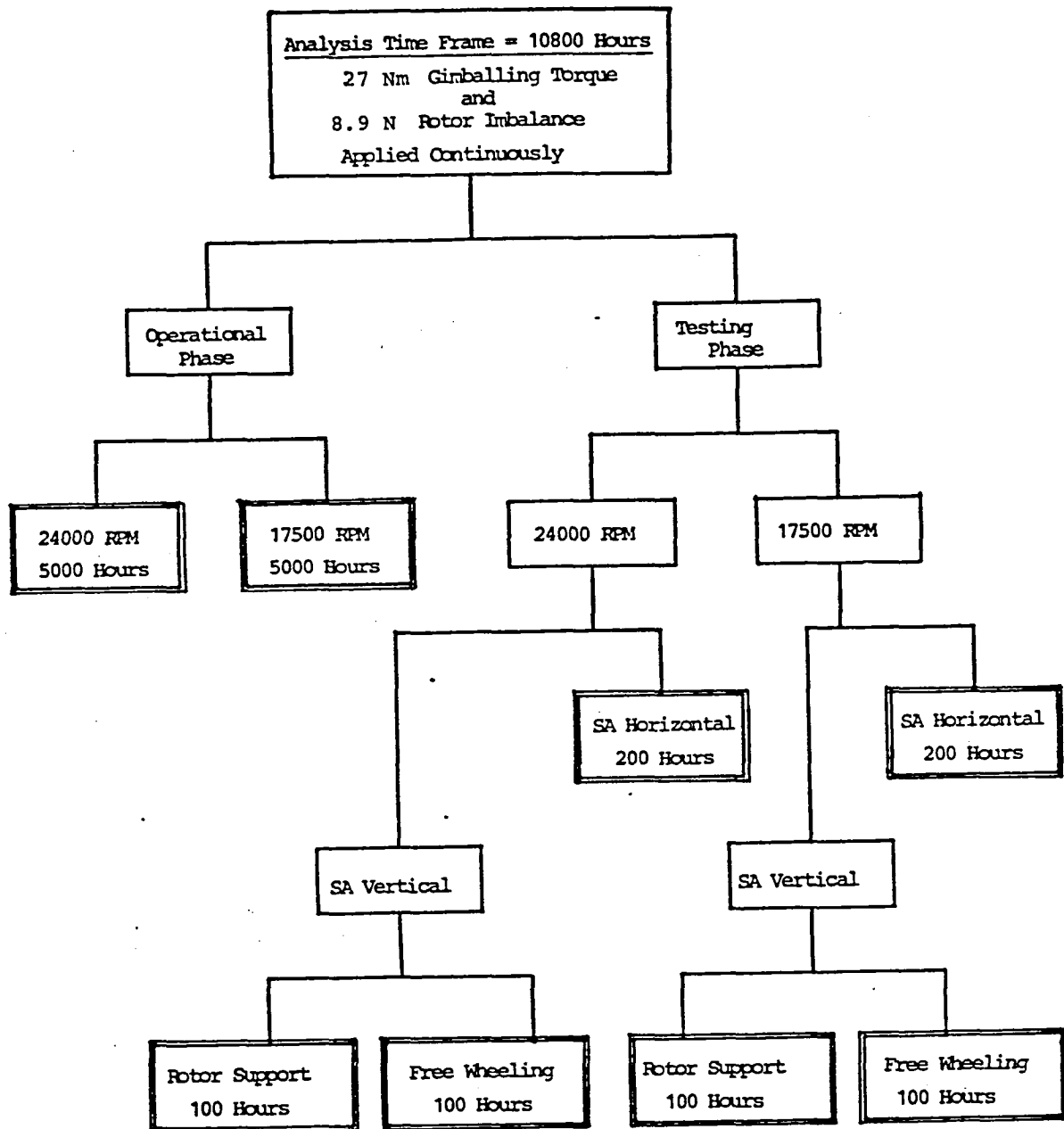
Figure 10.   Loading Case Breakdown for IPACS Spin Bearings

3.3.0 Inner Gimbal Analysis

The stress analysis performed on the IPACS inner gimbal is presented in the following sections. Vacuum, launch and gimballing loading conditions are described as they were applied to the finite element model. Stress and buckling factors and margins of safety are presented along with the stiffnesses of the inner gimbal structure.

3.3.1 Inner Gimbal Material

The inner gimbal is machined out of the aluminum alloy 6061, conforming to the government specification QQ-A-225/8. This designation applies to rolled, drawn or cold finished bar, rod, wire and special shapes. 6061 uses magnesium and silicon as the primary alloying elements. It has moderate strength and possesses excellent corrosion resistance and high fracture toughness.

The T651 temper is called out on the gimbal machining drawings but is modified in a note to the effect that the final mechanical properties of the material must meet or exceed those of the same alloy in a T6 temper. The T6 temper is a solution treat and age process; the T651 temper is the same as the T6, but is stress relieved by plastic stretching. Yield strength for the alloy is 241 MPa (35 ksi) while the ultimate strength is 289 MPa (42 ksi), (Reference 3). Other pertinent material properties are presented in Table VII.

Table VII. Inner Gimbal Material Data

Material :	6061 T651 Aluminum Alloy
Ultimate Strength :	289 MPa (42 ksi)
Yield Strength :	241 MPa (35 ksi)
Poisson's Ratio :	0.33
Modulus of Elasticity :	6.82×10^4 MPa (9.9×10^6 psi)
Density :	2715 kg/m^3 (0.098 lbs/in^3)
Fracture Toughness :	29.1 MPa.m$^{0.5}$ (26.5 ksi.in$^{0.5}$)

3.3.2 Inner Gimbal Finite Element Model

The inner gimbal of the IPACS was developed with an interactive computer modelling program and analyzed with NASTRAN. The model is constructed in 15° sectors, with 2118 nodes and 1208 solid hexahedral elements required to create the entire 360° structure (Figure 11).
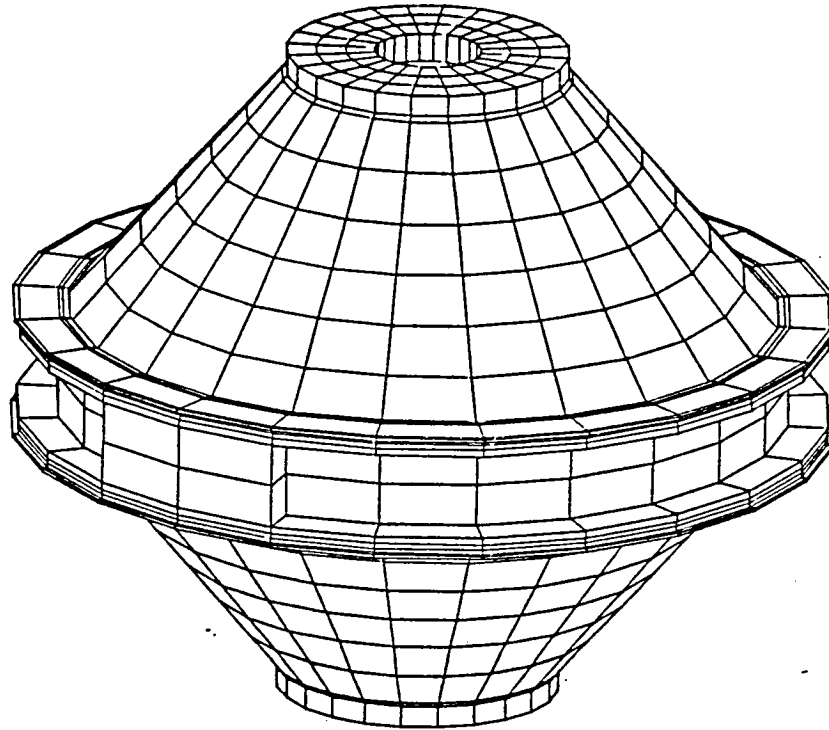
Figure 11. Inner Gimbal Finite Element Model

There are five primary pieces that make up the inner gimbal assembly. Two diametrically opposed mounting pads are bolted to the center gimbal ring where the gimbal pivots are attached. Two conically shaped, thin-shelled housing structures bolt to the center gimbal ring. These housing structures support the rotor assembly and transmit all launch and gimballing loads from the rotor to the gimbal ring and pivots. Because the webs of the housing structure are load bearing they are fairly thick at 2.4 mm (0.095 inch)..

Loads developed by the rotor are applied to the inside surface of the small ends of the housing structures where the bearing assemblies would reside. The model is supported rigidly at the two mounting pads with all degrees of freedom at the attachment points fixed to ground. Significant data about the model are presented in Table VIII.

Table VIII. Inner Gimbal Finite Element Model Data

Nodes:	2118
Elements:	1208 Solid Hexahedrals
Weight:	8.4 kg (18.5 lbs.)
Radius:	0.26 m (10.24 inches)
Height:	0.4237 m (16.68 inches)

Inertia about X axis (IA) = 0.255 $kg.m^2$ = 0.188 $ft.lbs.sec^2$
Inertia about Y axis (OA) = 0.309 $kg.m^2$ = 0.228 $ft.lbs.sec^2$
Inertia about Z axis (SA) = 0.346 $kg.m^2$ = 0.255 $ft.lbs.sec^2$

3.3.3 Loading Conditions

The IPACS inner gimbal system was analyzed for stresses during testing, launch, and operation. The internal vacuum necessary to test the system on earth is a significant loading condition and was modeled as a 0.101 MPa (14.7 psi) external pressure. This is not an operational loading condition as the system would be vented to the vacuum of outer space and no pressure differential across the housings would exist.

A launch vibration environment of 9.6 g's rms was applied to simulate an STS launch (solid plus liquid rockets). "G" loadings for all of the IPACS components are presented in the system response section. Accelerations are given along the three system axes: spin axis (SA), inner gimbal axis (IA), and outer gimbal axis (OA). The highest launch stresses occur when the system is launched with both the outer gimbal axis and spin axis vertical. In this configuration (Figure 12) the rotor receives 10.6 g's of acceleration and the inner gimbal receives 9.2 g's.

Table IX. Inner Gimbal Loading Conditions

Earth Testing:
    External Pressure = 0.101 MPa (14.7 psi)

Launch:
    Launch along IA   : 11.8 g's on Rotor, 9.4 g's on IG
    Launch along SA   : 10.2 g's on Rotor, 10.3 g's on IG
    Launch along OA   : 10.6 g's on Rotor, 9.2 g's on IG
    Launch along OA & SA : 10.6 g's on Rotor, 9.2 g's on IG

Operational:
    27 Nm (20 ft.lbs.) of Gimballing Torque

Outer Gimbal
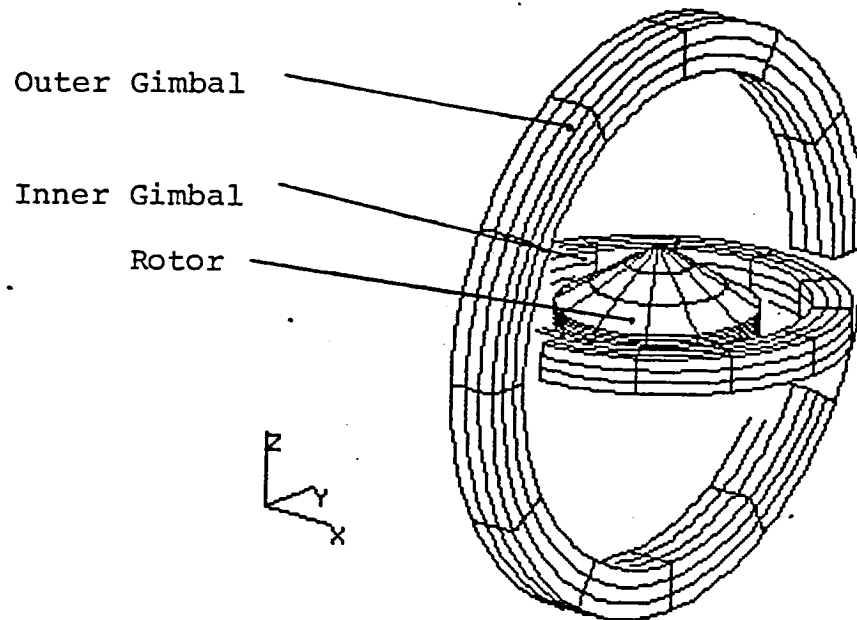
Inner Gimbal

Rotor

Representations of the structures are shown for clarity

Figure 12.   Inner Gimbal Loading Configuration

Operational loads on the inner gimbal consist solely of the 27 Nm (20 ft.lbs.) torque that is generated as the rotor is gimballed for attitude control. This loading case is very small at a maximum gimballing rate of 0.019 radians per second and produces stresses so low as to be insignificant. Loading conditions are summarized in Table IX.

3.3.4   Inner Gimbal Analysis and Results

Maximum stresses in each of the 6 loading conditions are compared to a yield strength of 241 MPa (35 ksi) for the 6061 aluminum alloy. Buckling failure modes were evaluated for each loading case and critical buckling loads were computed using techniques in References 5,6 and 7.

A vacuum within the IPACS inner gimbal system must be maintained during earth based testing so that high power losses due to windage do not occur. The maximum stress on the inner gimbal because of this 0.101 MPa (14.7 psi) external pressure is 18.0 MPa (2610 psi). This results in a high factor of safety of 13.4 (Margin of Safety=12.4). Buckling is another failure mode that was investigated. The critical external pressure required to produce buckling is 1.55 MPa (225 psi) versus the 0.101 MPa (14.7 psi) load case. The factor of safety for buckling is 15.3 (M.S.=14.3).

Launch induced stresses and factors of safety for the inner gimbal are presented in Table X.

Table X. Launch Stresses and Factors of Safety

Launch along IA	= 21.8 MPa (3160 psi)	F.S. = 11.0
Launch along SA	= 44.9 MPa (6520 psi)	F.S. = 5.4
Launch ·along OA	= 16.5 MPa (2390 psi)	F.S. = 14.6
Launch along OA & SA =	46.6 MPa (6760 psi)	F.S. = 5.2

The highest stress seen by the inner gimbal is 46.6 MPa (6760 psi) when the IPACS is launched with both the outer gimbal and spin axes vertical. Acceleration loads in this case are 10.6 g's for the rotor and 9.2 g's for the inner gimbal. The factor of safety for this worst case loading condition is a conservative 5.2.

Critical buckling loads and factors of safety for the launch environments are presented in Table XI.

Table XI. Launch Loads versus Critical Buckling Loads

Environment	Actual Load	Critical Load	F.S.
Launch along IA	3260 N 733 lbs.	234000 N 52500 lbs.	>>20
Launch along SA	5630 N 1265 lbs.	881000 N 198000 lbs.	>>20
Launch along OA	2930 N 658 lbs.	234000 N 52500 lbs.	>>20
Launch along OA & SA	5850 N 1315 lbs.	881000 N 198000 lbs.	>>20

Because of the thickness of the webs (2.4 mm or 0.095 inch) and the inherent stability of the conically formed housings, all factors of safety with respect to buckling are extremely high.

The operational loading environment that the inner gimbal sees is primarily that of the gimballing torque of 27 Nm (20 ft.lbs). This is equal to a maximum gimballing rate of 0.019 radians per second and produces stresses so low (<3.4 MPa (0.5 ksi)) as to be insignificant.

The inner gimbal is fairly stiff along all of the axes. This is due to the large flanges surrounding the central gimbal ring and the relatively thick webs (2.4 mm or 0.095 inch) of the conically shaped housings. These stiffnesses are presented below in Table XII.

<u>Table XII.   Inner Gimbal Stiffnesses</u>

Stiffness along X axis (IA) = 3.24×10^8 N/m
$\qquad\qquad\qquad\qquad\qquad$ (1.85×10^6 lbs/in)
Stiffness along Y axis (OA) = 4.52×10^8 N/m
$\qquad\qquad\qquad\qquad\qquad$ (2.58×10^6 lbs/in)
Stiffness along Z axis (SA) = 2.07×10^8 N/m
$\qquad\qquad\qquad\qquad\qquad$ (1.18×10^6 lbs/in)

Because the gimballing environment is so benign, the present inner gimbal design is quite adequate. Highest stresses occur during launch of the system but are very low at less than 20% of the yield strength of the 6061 aluminum alloy. The housing webs are fairly thick for such a short span and as a result the margins of safety with respect to buckling are very high.

3.4.0 Outer Gimbal Analysis

The stress analysis performed on the conceptual outer gimbal for the IPACS is described in the following sections. A one-eighth-section model was developed and loaded with those forces predicted in the systems analysis. Stresses and stiffnesses are presented in the results section.

3.4.1 Outer Gimbal Model and Material

The outer gimbal designed for the IPACS is an octagonal structure cast in A356.0 aluminum alloy. This alloy is strong, tough and has excellent fabrication characteristics. Data on this alloy are presented in Table XIII.

32

Table XIII. Outer Gimbal Material Data

Material = A356.0 Cast Aluminum Alloy
Ultimate Strength = 227 MPa (33 ksi)
Yield Strength   = 186 MPa (27 ksi)
Poisson's Ratio   = 0.33
Modulus of Elasticity = 7.16×10^4 MPa $(10.4 \times 10^6$ psi)
Density = 2685 kg/m^3 (0.097 lbs/in^3)
Fracture Toughness = 15.4 MPa.m$^{0.5}$ (14 ksi.in$^{0.5}$)

The model used to analyze the gimbal (Figure 13), takes advantage of the three planes of symmetry that occur in the design. A one-eighth section of the gimbal was modeled with 24 solid hexahedral elements, 42 quadrilateral plate elements and 123 grid points.
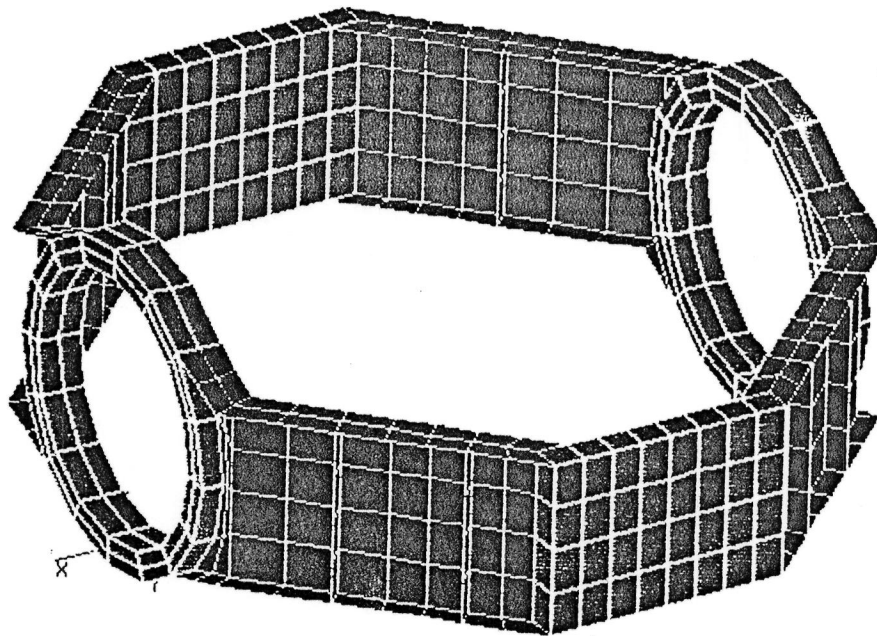

Figure 13. Outer Gimbal Finite Element Model

The bearing rings and pivot attachment sections are modeled
with the solid elements, while the webbed areas between
those sections are modeled with the plates. Spline elements
are used at the solid element/plate element boundaries to
properly transfer the bending moment between the sections.
Symmetrical /antisymmetrical boundary conditions are imposed
on the "cut" surfaces of the model to simulate the remainder
of the structure. Loads are applied to a grid point at the
center of the outer gimbal model. This grid point is
attached to the model with rigid body elements which
transfer the loads to the inner surface of the bearing ring.
Model data are presented in Table XIV.

Table XIV. Outer Gimbal Model Data

Nodes = 984
Elements = 656
Length = 0.686 m   (27.0 in.)
Width = 0.584 m   (23.0 in.)
Height = 0.279 m   (11.0 in.)
Weight = 12.7 kg (28.0 lbs.)
Moment of Inertia about SA =1.308 $kg.m^2$ (11.58 $in.lbs.sec^2$)
Moment of Inertia about IA =0.837 $kg.m^2$ (7.41 $in.lbs.sec^2$)
Moment of Inertia about OA =0.594 $kg.m^2$ (5.26 $in.lbs.sec^2$)

3.4.2 Outer Gimbal Loading Conditions

The outer gimbal was analyzed for stresses developed by the
worst case loading of a launch environment. A launch
environment of 9.6 g's rms was applied to the entire IPACS
to simulate an STS launch (solids plus liquid rockets).
Component loads for the IPACS are detailed in the System
Analysis section.

Operational loading of the outer gimbal involves the 27 Nm
(20 ft.lbs.) precession torque generated by torquing the
IGA. This condition develops stresses that are
insignificantly small, confirming the assumption that the
worst case environment for the outer gimbal is launch.

3.4.3 Outer Gimbal Analysis and Results

Maximum stresses developed during launch are extremely low,
and the stiffness of the structure is very high. Results
from the stress analysis are presented in Table XV.

Table XV. Outer Gimbal Stresses and Stiffnesses

Peak Launch Stress = 3.6 MPa   (520 psi)
Yield Strength of A356.0 = 186 MPa   (27 ksi)
Factor of Safety $>$ 50

Stiffness along IA = 2.00×10^8 N/m   (1.14×10^6 lbs/in)
Stiffness along OA = 2.19×10^8 N/m   (1.25×10^6 lbs/in)
Stiffness along SA = 1.28×10^8 N/m   (7.33×10^5 lbs/in)

Factors of safety on stress are very high for this conceptual design, indicating that structural modifications for weight reduction would be advantageous in a detailed design and build effort. The stiffnesses are high insuring small operating deflections and contributing to precise loop control. For these reasons, the outer gimbal design is considered to be more than adequate for the intended application.

3.5.0 Mounting Ring Analysis

The stress analysis for the conceptual mounting ring structure is quite similar to the outer gimbal analysis, and will be detailed in the following sections. The system response analysis provides the loads that were applied to a one-quarter-section finite element model of the mounting ring. Stresses and stiffnesses are presented in the results section.

3.5.1 Mounting Ring Model and Material

The mounting ring designed for the IPACS is an octagonal structure cast in A356.0 aluminum alloy, much the same as the outer gimbal. Property data for this alloy are shown in Table XIII.

The model used to analyze the mounting ring (Figure 14), takes advantage of two planes of symmetry, so only a one-quarter section of the structure need be modeled. A total of 36 solid hexahedral elements, 218 plate elements and 301 grid points define the geometry of the model. Modelling techniques and assumptions are identical to those previously described in the outer gimbal model section (Section 3.4.1).
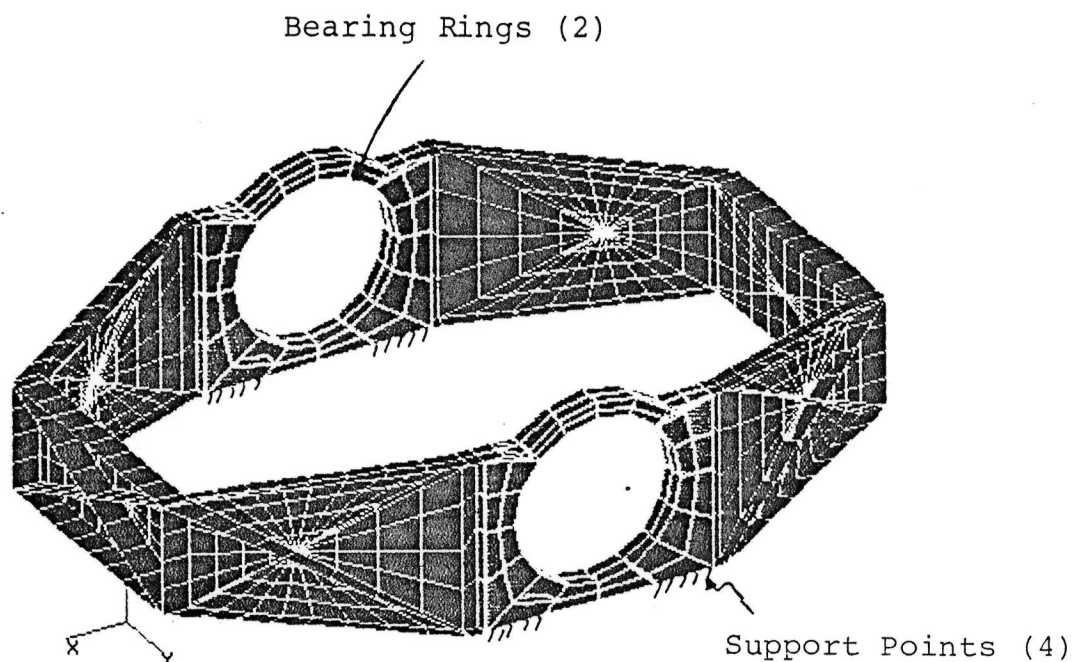
Figure 14. Mounting Ring Finite Element Model

Important data describing the mounting ring model are presented in Table XVI.

Table XVI. Mounting Ring Model

```
            Nodes = 1204
            Elements = 1068
            Length = 1.01 m    (39.65 in.)
            Width = 0.711 m    (28.0 in.)
            Height = 0.279 m   (11.0 in.)
            Weight = 13.1 kg   (29.0 lbs.)
Moment of Inertia about SA =3.494 kg.m²  (30.92 in.lbs.sec²)
Moment of Inertia about IA =1.715 kg.m²  (15.18 in.lbs.sec²)
Moment of Inertia about OA =2.020 kg.m²  (17.88 in.lbs.sec²)
```

36

3.5.2 Mounting Ring Loading Conditions

Launch loads for the mounting ring were predicted in the systems response analysis section. These loads were developed from an STS launch environment of 9.6 g's rms. Operational loading of the mounting ring is the negligible (from a stress point of view) 27 Nm (20 ft.lbs) of output torque.

3.5.3 Mounting Ring Analysis and Results

Maximum stresses developed during launch are very small and the structural stiffnesses are quite high. Results of the stress analysis are presented in Table XVII.

Table XVII. Mounting Ring Stresses and Stiffnesses

Peak Launch Stress $<$ 3.4 MPa (500 psi)
Factor of Safety $>$ 50

Stiffness along IA = 5.88×10^9 N/m (3.36×10^7 lbs/in)
Stiffness along SA = 4.04×10^9 N/m (2.31×10^7 lbs/in)
Stiffness along OA = 1.75×10^{10} N/m (1.00×10^8 lbs/in)

As in the case of the outer gimbal, the very low stresses and very high stiffnesses suggest that important reductions in weight could be achieved in a more detailed effort. Because of the relatively mild loading applied to the mounting ring, this design is considered to be more than adequate for the intended application.

4.0 Thermal Analysis

A computer thermal analysis was performed for the IPACS IGA with several goals in mind. Although it was clear that the maximum operating speed of the rotor should be restricted to 24000 rpm, several analyses were run at 35000 rpm. This was done so that the results reported in Reference 1 might be verified and also to study the performance characteristics between the heat pipe and a solid copper rod. A worst case loading condition at 24000 rpm was also analyzed to predict actual operational temperatures. The following sections will detail the computer model, various loading conditions and the results of the analyses.

4.1 Thermal Model

Forty-one nodes are used to describe one half of the cross section of the IPACS IGA. External heat rejection is by conduction to the mounting bracket and free convection and radiation to the environment. Because the worst case thermal loadings occur on earth during testing, the external environment of the IGA is sea level air at 294° K (70° F) and the gimbal mounting structure is set at 294° K (70° F). Heat transfer coefficients were calculated and input to the computer program along with the source power inputs and the sink temperatures. Nodal designations for the thermal model can be found in Figure 15 and Table XVIII.

Table XVIII.   IPACS IGA Thermal Model Nodal Designations

Node	Description
1	Bearing, Inner Race, Upper
2	Bearing, Outer Race, Upper
3	Shaft Plug, Upper
4	Heat Pipe, Upper
5	Bearing Sleeve
6	Bearing Sleeve Housing
7	Preload Housing
8	End Plate Cover, Upper
9-10	Inner Gimbal Housing Cover, Upper
11	Motor/Generator Rotor, Upper
12	Motor/Generator Stator, Upper
13	Motor/Generator Housing, Upper
14-18	Wheel, Upper Half
19	Clamp Ring, Upper
20	Inner Gimbal Ring
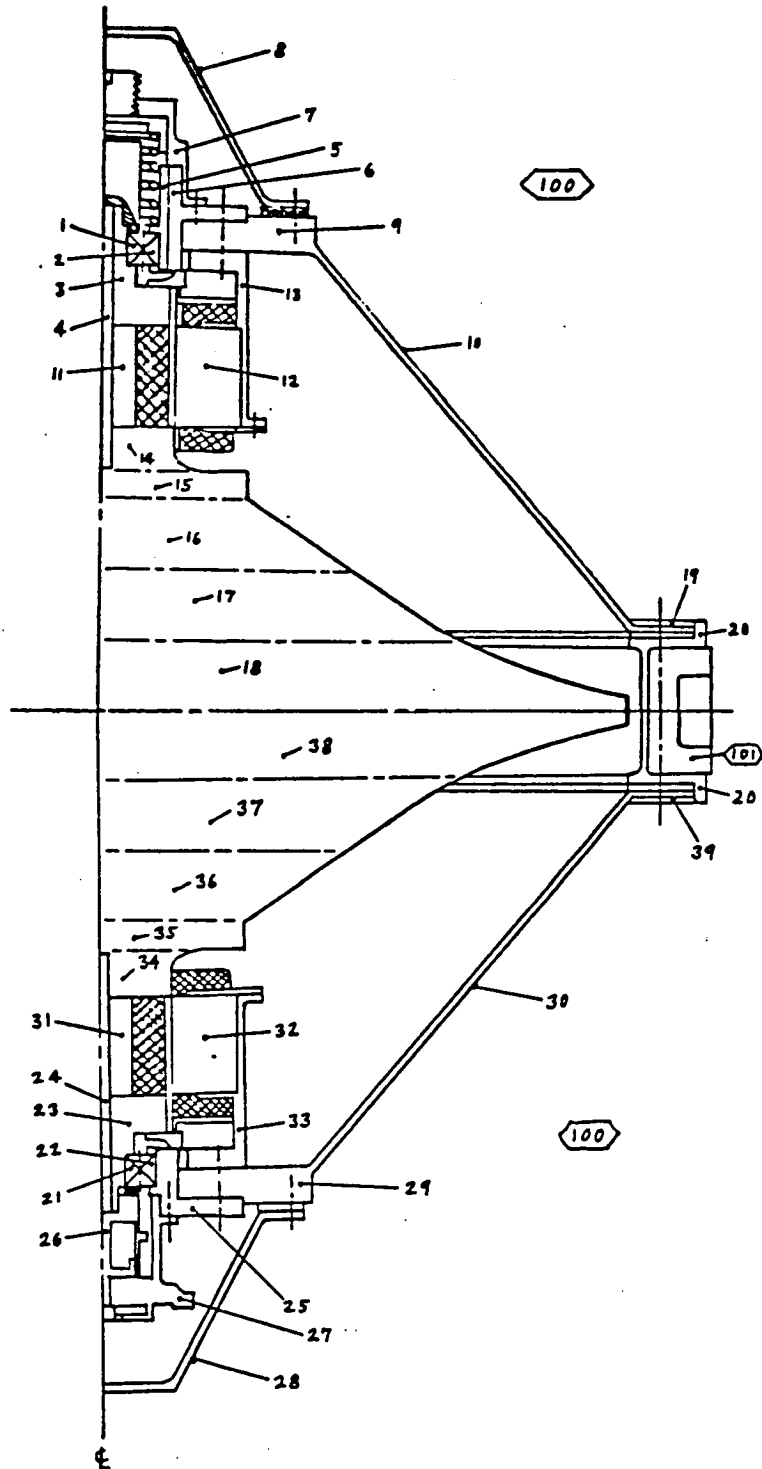
Figure 15. IPACS IGA Thermal Model Node Designations

21	Bearing, Inner Race, Lower
22	Bearing, Outer Race, Lower
23	Shaft Plug, Lower
24	Heat Pipe, Lower
25	Bearing Housing
26	Oiler Assembly
27	Sensor Housing
28	End Plate Cover, Lower
29-30	Inner Gimbal Housing Cover, Lower
31	Motor/Generator Rotor, Lower
32	Motor/Generator Stator, Lower
33	Motor/Generator Housing, Lower
34-38	Wheel, Lower Half
39	Clamp Ring, Lower
100	Environment
101	Mounting Bracket

4.2 Thermal Loading Condition

One analysis was performed to verify the results contained
in Reference 1. Operating speed was 35000 rpm, SA
horizontal, 67 N (15 lbs) preload, on earth operation with
inner cavity evacuated, 22 watts power dissipation per spin
bearing and 1.2 watts of power per motor/generator stator.
Two other analyses were also performed at 35000 rpm to
investigate the performance of the heat pipe currently in
the IPACS IGA with a simpler solid copper rod. Spin bearing
power was increased to 27.3 watts per the spin bearing drag
torque analysis (see Section 3.2). Finally, a fourth
analysis was performed to predict worst case operating
temperatures. This load case was defined at 24000 rpm, SA
vertical, on earth operation, 67 N (15 lbs) preload, with a
drag torque power dissipation of 10 watts for the upper spin
bearing, 66 watts for the lower spin bearing and stator
powers of 1.4 watts apiece. The windage power of 0.026
watts/cm^2 of rotor surface, at 35000 rpm and 2 microns of
internal pressure, was neglected in this analysis.
Experience has shown that windage levels of this size do not
significantly alter the thermal analysis results.

4.3 Thermal Analysis Results

Inspection of the results from the verification analysis,
(Table XIX), indicates that the current analysis diverges
from the original analysis with respect to one analytical
assumption. The original analysis applied 85% of the spin
bearing drag torque power to the inner race and 15% to the

outer race. Extensive testing has shown that this power split is closer to 50%-50% as is applied in the current analysis. For this reason, the rotating assembly components in the current analysis are generally cooler and the stationary components generally warmer than those values predicted originally. Furthermore, the closer the component is to the bearing, the greater this discrepancy is. It is instructive to note that the overall average bearing temperatures are quite similar, indicating that the models are analogous. Operational testing would be required to validate either of the analyses.

Table XIX. Thermal Model Comparison Analysis

Load Case: 35000 rpm, SA horizontal, on earth operation with inner cavity evacuated to 2 microns on internal pressure, 67 N (15 lbs) preload, 22 watts power dissipation per spin bearing and 1.2 watts of power per motor/generator stator.

Node	Bendix Results $^\circ K$	$^\circ F$	Rockwell Results $^\circ K$	$^\circ F$
1	340	153	379	222
2	340	152	315	108
3	315	107	364	196
4	313	104	363	194
5	320	116	–	–
6	319	115	–	–
7	316	109	323	122
8	302	84	299	79
9	304	88	311	100
10	300	80	309	97
11	313	104	353	176
12	314	106	320	117
13	304	88	–	–
14	307	93	350	170
15	306	92	344	160
16	305	90	340	152
17	305	90	342	156
18	305	90	341	155
19	299	79	–	–
20	299	78	–	–
100	294	70	294	70
101	294	70	294	70

A comparison of the temperatures for the heat pipe model and the copper rod model indicate that there is no significant

difference in performance. This is due to the fact that the limiting thermal resistance is at the titanium-nickel boundary between the rotor and the heat pipe/copper rod. Because both configurations contain this boundary resistance, both act similarly, and there is a valid case for consideration of the simpler copper rod over the heat pipe design.

The analytical results from the worst case thermal loading analysis, (Table XX), predict a maximum temperature at the bearings of about 396° K (253° F). This temperature is handled easily by the M-50 tool steel spin bearings currently in the system and is also well within the capabilities of the more standard and cheaper VIM VAR 52100 bearing steel.

Table XX. Worst Case Thermal Loading Analysis Results

Load Case: 24000 rpm, SA vertical, on earth operation with inner cavity evacuated to 2 microns of internal pressure, 67 N (15 lbs) preload, with a drag torque power dissipation of 10 watts for the upper spin bearing, 66 watts for the lower spin bearing, and stator powers of 1.4 watts apiece.

Node	°K	°F	Node	°K	°F
1	321	118	22	393	248
2	320	117	23	335	144
3	314	105	24	332	138
4	313	104	25	367	201
5	310	99	26	344	159
6	310	99	27	350	170
7	309	96	28	314	105
8	301	82	29	320	117
9	303	86	30	305	90
10	301	82	31	332	138
11	313	104	32	326	128
12	316	109	33	318	113
13	304	87	34	316	110
14	311	101	35	314	106
15	311	100	36	312	102
16	311	100	37	311	101
17	311	100	38	311	100
18	311	100	39	305	89
19	301	82	100	294	70
20	301	83	101	294	70
21	396	253			

5.0 System Response Analysis

The loading on any component of a structural system depends upon the interaction of all of the components in the system. Each component actively participates in the damping or amplification of the loading environment as it propagates through the system. For this reason, a system response analysis was performed on the IPACS package to determine the maximum loading conditions in a launch environment. The mathematical model describing the IPACS, the loading environment applied to the model, and the resultant launch loads will be discussed in the following sections.

5.1 IPACS Spring/Mass Model

A seven degree of freedom model was used to describe the IPACS. The model is a single path model in that there are no nodes that have more than two elements (1 mass, 1 spring) connected to it. The central mass in the system is the rotor, weighing 54 kg. (119 lbs).

$$\text{Mass 1} = \text{Rotor} = 54 \text{ kg.}\quad (119 \text{ lbs.})$$

The rotor is supported by the stiffness of the motor/generator housings. Their spring rates were computed from the Rotor Analysis.

$$
\begin{aligned}
\text{Spring 1} = \text{Motor Housings} &= 6.46 \times 10^8 \text{ N/m along SA} \\
&\quad (3.69 \times 10^6 \text{ lbs/in}) \\
&= 5.74 \times 10^9 \text{ N/m laterally} \\
&\quad (3.28 \times 10^7 \text{ lbs/in})
\end{aligned}
$$

The spin motor rotors, rotor shafts, bearing inner races and the spin bearing lube systems are grouped into the second mass,

$$\text{Mass 2} = \text{Motor/Shaft} = 4.54 \text{ kg}\quad (10 \text{ lbs.})$$

which is supported by the spin bearings, preloaded to 67 N (15 lbs).

$$
\begin{aligned}
\text{Spring 2} = \text{Spin Bearings} &= 2.70 \times 10^7 \text{ N/m Axially} \\
&\quad (1.54 \times 10^5 \text{ lbs/in}) \\
&= 1.60 \times 10^8 \text{ N/m Radially} \\
&\quad (9.17 \times 10^5 \text{ lbs/in})
\end{aligned}
$$

The inner gimbal structure was split between masses 3 and 4.

```
Mass 3 = 1/2 Inner Gimbal + Motor stators + misc
       = 9.15 lbs. + 17.8 lbs. + 4.65 lbs.
       = 4.15 kg.  + 8.07 kg.  + 2.11 kg.
       = 14.33 kg.

Mass 4 = 1/2 Inner Gimbal + 1/2 Inner Pivots
       = 9.15 lbs. + 35.0 lbs.
       = 4.15 kg.  + 15.88 kg.
       = 20.03 kg.
```

These two masses (3 and 4) are connected in the model by spring 3, the stiffness of the inner gimbal. Estimates of the stiffness of the inner gimbal are:

$$\text{Spring 3} = \text{Inner Gimbal} = \text{Along SA} = 3.50 \times 10^8 \text{ N/m}$$
$$(2.0 \times 10^6 \text{ lbs/in})$$

$$= \text{Along IA} = 3.50 \times 10^8 \text{ N/m}$$
$$(2.0 \times 10^6 \text{ lbs/in})$$

$$= \text{Along OA} = 3.50 \times 10^7 \text{ N/m}$$
$$(2.0 \times 10^5 \text{ lbs/in})$$

The interface between the inner and outer gimbals is the inner pivots. Modeled as spring 4, the stiffnesses used are:

$$\text{Spring 4} = \text{Inner Pivots} = \text{Along SA} = 5.25 \times 10^8 \text{ N/m}$$
$$(3.0 \times 10^6 \text{ lbs/in})$$

$$= \text{Along IA} = 1.75 \times 10^8 \text{ N/m}$$
$$(1.0 \times 10^6 \text{ lbs/in})$$

$$= \text{Along OA} = 5.25 \times 10^8 \text{ N/m}$$
$$(3.0 \times 10^6 \text{ lbs/in})$$

The outer gimbal structure is split between the model's mass elements 5 and 6. The estimated outer gimbal weight is 9.1 kg (20 lbs).

```
Mass 5 = 1/2 Outer Gimbal + 1/2 Inner Pivots
       = 10.0 lbs. + 35.0 lbs.
       = 4.54 kg.  + 15.88 kg.
       = 20.42 kg.

Mass 6 = 1/2 Outer Gimbal + 1/2 Outer Pivots
       = 10.0 lbs. + 35.0 lbs.
       = 4.54 kg.  + 15.88 kg.
       = 20.42 kg.
```

Spring 5 is between these two masses,

Spring 5 = Outer Gimbal = Along SA = 3.50×10^8 N/m
(2.0×10^6 lbs/in)

= Along IA = 1.75×10^8 N/m
(1.0×10^6 lbs/in)

= Along OA = 8.76×10^7 N/m
(5.0×10^5 lbs/in)

while spring 6 (the outer pivots) follows them.

Spring 6 = Outer Pivots = Along SA = 5.25×10^8 N/m
(3.0×10^6 lbs/in)

= Along IA = 5.25×10^8 N/m
(3.0×10^6 lbs/in)

= Along OA = 1.75×10^8 N/m
(1.0×10^6 lbs/in)

The final mass element in the model includes half the
mounting frame, (frame weight estimate = 50.3 kg,(25 lbs.)),
and half the outer pivot weight.

Mass 7 = 1/2 Mounting Frame + 1/2 Outer Pivots
= 12.5 lbs. + 35.0 lbs.
= 5.67 kg. + 15.9 kg.
= 21.5 kg.

This mass is attached to ground via spring 7; which is the
estimated mounting frame stiffnesses.

Spring 7 = Mounting Frame = Along SA = 1.75×10^8 N/m
(1.0×10^6 lbs/in)

= Along IA = 8.76×10^7 N/m
(5.0×10^5 lbs/in)

= Along OA = 8.76×10^7 N/m
(5.0×10^5 lbs/in)

Half of the frame weight is included in the infinite mass of
the ground and is implicitly accounted for. The total
weight of the system is expected to be around 716 kg
(355 lbs). Mass and spring values are tabulated in
Table XXI and the model schematic is shown in Figure 16.

Mass 1 = Rotor

Spring 1 = Motor/Generator Housings

Mass 2 = Spin Motor Rotors + Rotor Shafts + Bearing Inner Races + Lube Systems

Spring 2 = Spin Bearings

Mass 3 = 1/2 Inner Gimbal + Motor Stators + Misc.

Spring 3 = Inner Gimbal

Mass 4 = 1/2 Inner Gimbal + 1/2 Inner Pivots

Spring 4 = Inner Pivots

Mass 5 = 1/2 Outer Gimbal + 1/2 Inner Pivots

Spring 5 = Outer Gimbal

Mass 6 = 1/2 Outer Gimbal + 1/2 Outer Pivots

Spring 6 = Outer Pivots

Mass 7 = 1/2 Mounting Frame + 1/2 Outer Pivots
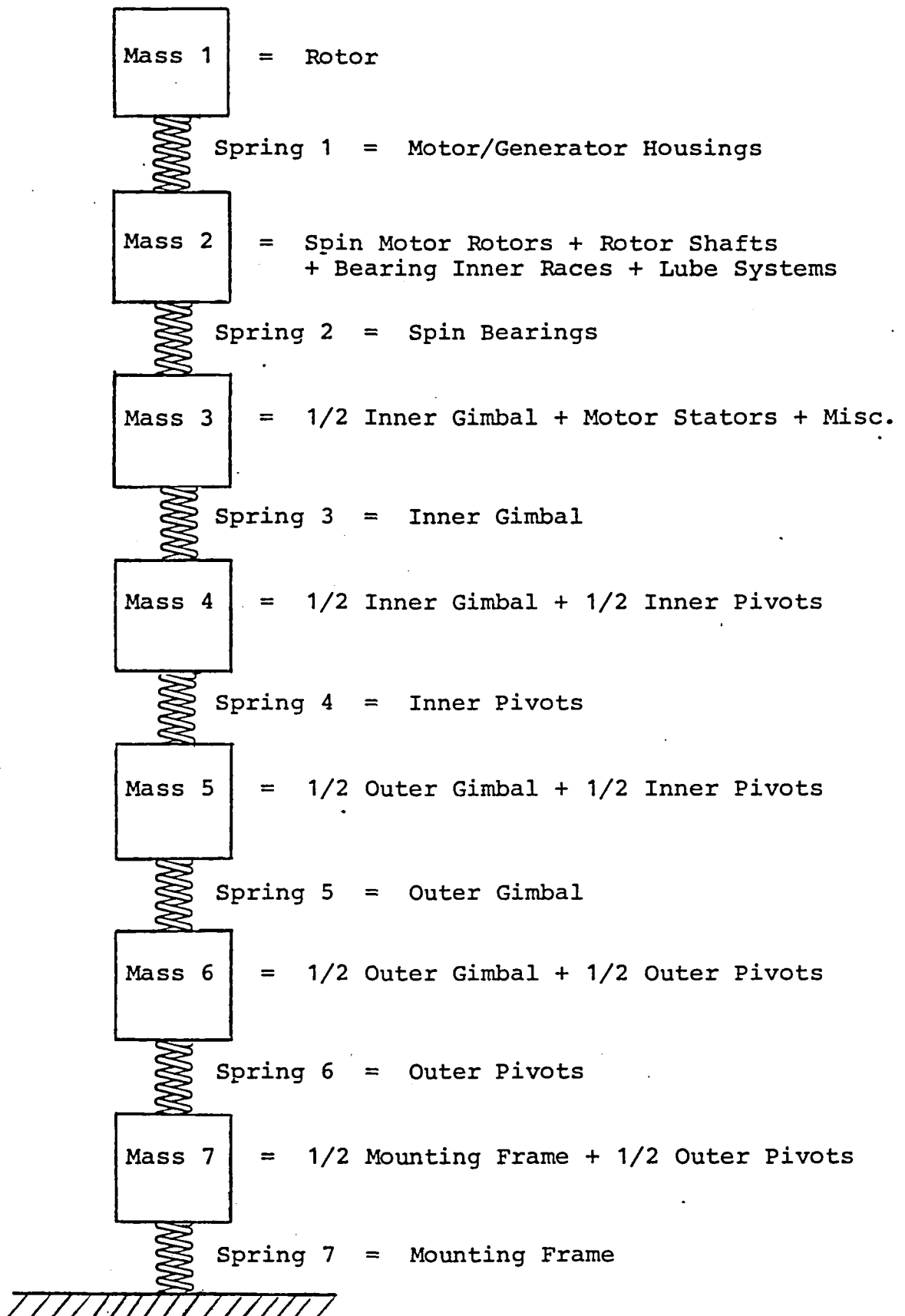
Spring 7 = Mounting Frame

Figure 16. IPACS Model for the System Response Analysis

Table XXI. Spring and Mass Values for the System Response Model

Body	Mass	Stiffness		
	kg ($lbs.sec^2/in$)	Along IA 10^8 N/m (10^6 lbs/in)	Along OA 10^8 N/m (10^6 lbs/in)	Along SA 10^8 N/m (10^6 lbs/in)
1	54.0 (0.308)	57.4 (32.8)	57.4 (32.8)	6.46 (3.69)
2	4.54 (0.0259)	1.60 (0.92)	1.60 (0.92)	0.27 (0.15)
3	14.33 (0.0818)	3.50 (2.0)	0.35 (0.20)	3.50 (2.0)
4	20.03 (0.114)	1.75 (1.0)	5.25 (3.0)	5.25 (3.0)
5	20.42 (0.116)	1.75 (1.0)	0.88 (0.50)	3.50 (2.0)
6	20.42 (0.116)	5.25 (3.0)	1.75 (1.0)	5.25 (3.0)
7	21.5 (0.123)	0.88 (0.50)	0.88 (0.50)	1.75 (1.0)

5.2 Launch Environments

Three launch environments were applied to the IPACS spring-mass model: 1) the original Skylab launch at 4.6 g's rms; 2) the final or high level Skylab launch (liquid rocket) at 5.2 g's rms; and 3) an STS launch (solids plus liquid rockets) at 9.6 g's rms. This final environment is the most severe and produces the highest component loads in the system analysis. A spectral density plot of the STS launch vibration environment is presented in Figure 17.
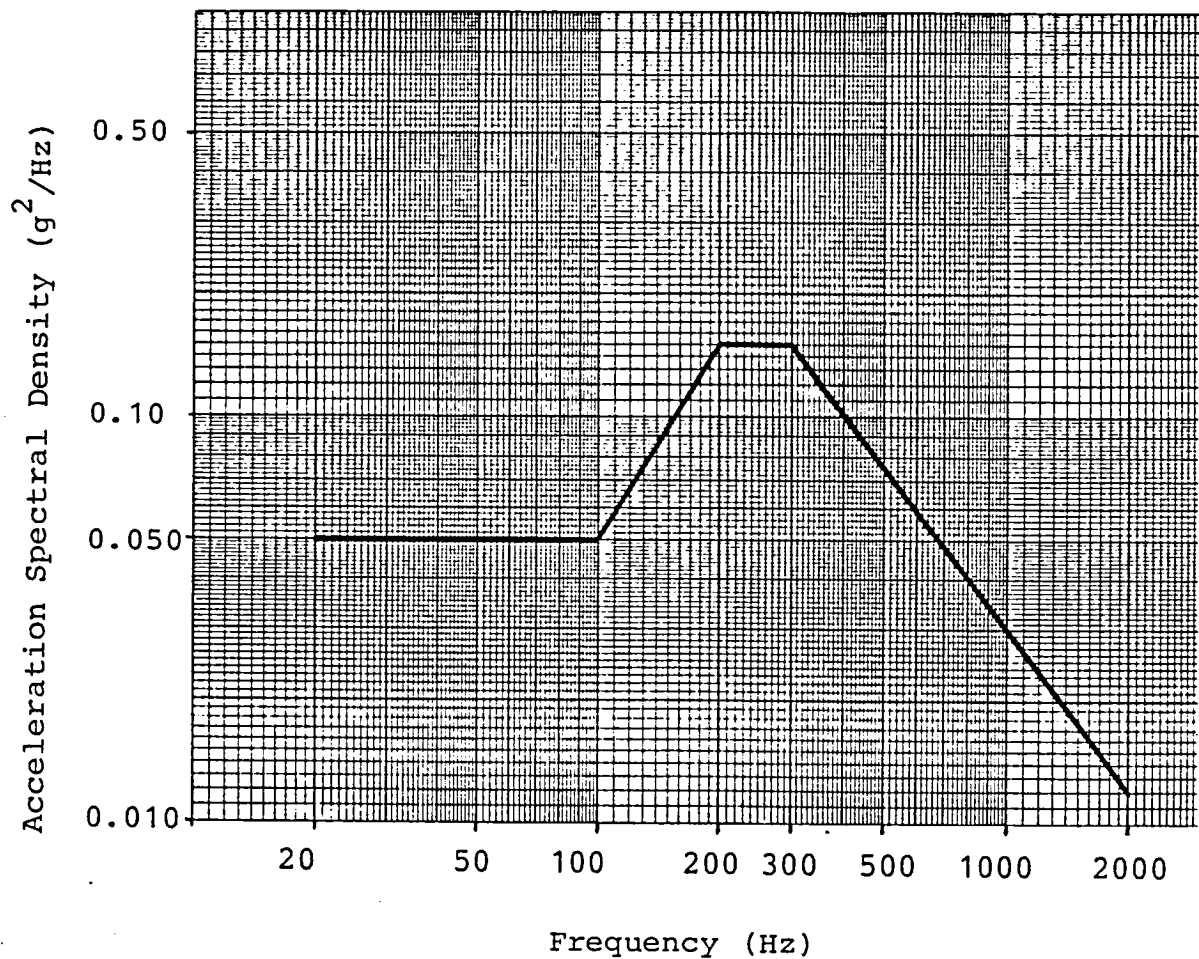
Figure 17. Spectral Density Plot of STS Launch Vibration Environment

5.3 Launch Loads

The highest loads developed in the system are tabulated in Table XXII. These loads are comfortably within the capabilities of the current system as is indicated by the large factors of safety predicted in the structural analyses (see Section 3). System response analysis is an iterative procedure and in a phase II effort, optimization and detailing of the component structures would necessitate updating this model and analysis.

48

Table XXII. System Response Analysis Results

Maximum Design Loads (1σ)

Body	Along IA N (lbs)	Along OA N (lbs)	Along SA N (lbs)
1	6230 (1400)	5600 (1260)	5380 (1210)
2	6760 (1520)	6090 (1370)	5830 (1310)
3	7870 (1770)	7340 (1650)	6270 (1410)
4	9210 (2070)	7830 (1760)	7290 (1640)
5	10230 (2300)	8940 (2010)	8580 (1930)
6	11120 (2500)	9700 (2180)	8980 (2020)
7	12230 (2750)	10500 (2360)	10850 (2440)

6.0 Conclusions

Gimballing the IPACS IGA is easily accomplished owing to the benign gimballing environment of 27 Nm (20 ft.lbs.) of torque. However, modifications to the IGA are required to transform the system from its current laboratory concept phase to a realistic flight hardware status.

The most critical modification that must be made is the reduction in the top speed of the rotor from 35000 rpm to 24000 rpm. This constraint must exist in order to prevent crack growth at the center of the rotor from developing into brittle fracture. Unfortunately, there is a considerable loss in power storage capability due to this speed reduction. The original discharge cycle of 35000 rpm to 17500 rpm generated 2200 watts of power, while the proposed 24000 rpm to 12000 rpm discharge cycle will generate less than half of that at 1040 watts. Some of this may be regained by investigating materials with higher strength to weight ratios than the 6Al-4V titanium currently being used. Two such metals would be Custom 455 stainless steel and B120 VCA titanium. Additionally, the maximum torquing rate would have to be increased to about 0.028 radians per second at 12000 rpm to produce the required 27 Nm (20 ft.lbs.) of output torque. As this is still a very mild gimballing environment, it would not be expected to adversely affect the performance of the IPACS.

Another important modification is to upgrade the current preloading mechanism to a bellville washer system. Significant reductions in drag torque power could be achieved by switching to this method of preloading (see Section 3.2). Not only would the efficiency of the IPACS be enhanced, but reliability of the system would increase due to the cooler operating environment of the IGA.

Currently, the IPACS spin bearings are made of M50 tool steel for improved high temperature operation and fatigue life. With the speed reduction to 24000 rpm, this exotic high cost material is no longer necessary and the use of standard VIM VAR 52100 bearing steel would be more desirable.

To promote spin bearing stability, bearing retainer design should be investigated. Bearing stability is extremely important and its effects are influential throughout the system's performance.

50

7.0 References

1. Cormack,A. III; and Notti,J.E.: "Design Report for the Rotating Assembly for an Integrated Power /Attitude Control System", NASA CR-172317, September 1974.

2. Applied Elasticity, C. Wang, McGraw Hill Book Company, 1953.

3. MIL-HDBK-5C, "Military Standardization Handbook - Metallic Materials and Elements for Aerospace Vehicle Structures", 1978.

4. Jones,A.B.: "High Speed Ball Bearing Analysis Program", A.B.Jones, 37 Birchlawn Terrace, Newington, Connecticutt 06111; 1982.

5. Seide,P. and Weingarten,V.I.: "On the Buckling of Circular Cylindrical Shells under Pure Bending", ASME Paper no. 60-WA-33; March 1961.

6. Jahsman,W.E.: "Combined Bending and Compression of a Pressurized Circular Cylindrical Membrane Column", ASME Paper no. 64-WA/AV-2, August 1964.

7. Formulas for Stress and Strain, R.Roark and W.Young; Fifth Edition, McGraw Hill, 1975.

1. Report No. NASA CR-172524	2. Government Accession No.	3. Recipient's Catalog No.
4. Title and Subtitle The Gimbal Sizing Analysis for an IPACS Rotating Assembly		5. Report Date May 1985
		6. Performing Organization Code
7. Author(s) P.A.Coronato and P.R.Burke		8. Performing Organization Report No.
9. Performing Organization Name and Address Allied Bendix Aerospace Route 46 Teterboro, New Jersey 07608		10. Work Unit No.
		11. Contract or Grant No. NAS 1-17658
12. Sponsoring Agency Name and Address National Aeronautics and Space Administration Washington, D.C. 20546		13. Type of Report and Period Covered Contractor Report
		14. Sponsoring Agency Code 506-57-13-01

15. Supplementary Notes

Technical Monitor: Claude R. Keckler, NASA-Langley Research Center

16. Abstract

This report presents the Gimbal Sizing Analysis for an IPACS Rotating Assembly. All major components of the assembly were analyzed for testing, launch, and operational stresses. The conceptual design for the outer gimbal and mounting ring structures were developed and analyzed along with preliminary designs of the pivot and torquer assemblies. Results from the system response analysis and the thermal analysis are also presented. Gimballing of this rotating assembly should present few difficulties as the maximum gimballing rate is quite low. However, the inner gimbal assembly in its current configuration must be modified to develop the system from a laboratory concept to a realistic flight hardware status.

17. Key Words (Suggested by Author(s)) IPACS, Gimballing, Plasticity Power Storage, Control Moment Gyro (CMG)	18. Distribution Statement Unclassified- Unlimited Subject Category 20

19. Security Classif. (of this report) Unclassified	20. Security Classif. (of this page) Unclassified	21. No. of Pages 55	22. Price

N-305